Arabidopsis RETINOBLASTOMA RELATED directly regulates DNA damage responses through functions beyond cell cycle control

Beatrix M. Horvath[1,2,#,*], Hana Kourova[3,#], Szilvia Nagy[4], Edit Nemeth[1], Zoltan Magyar[5], Csaba Papdi[1], Zaki Ahmad[1], Gabino F. Sanchez-Perez[2], Serena Perilli[6], Ikram Blilou[6], Aladár Pettkó-Szandtner[5], Zsuzsanna Darula[7], Tamas Meszaros[4,8], Pavla Binarova[3], Laszlo Bogre[1,9] and Ben Scheres[2,6,9*]

[1]School of Biological Sciences, Centre for Systems and Synthetic Biology, Royal Holloway, University of London, Egham Hill, Egham, TW20 0EX, UK

[2]Department of Molecular Genetics, Utrecht University, 3584 CH Utrecht, The Netherlands

[3]Institute of Microbiology ASCR, v.v.i. Laboratory of Functional Cytology, Vídeňská 1083 Prague 4, 14 200, Czech Republic

[4]Department of Medical Chemistry, Molecular Biology and Pathobiochemistry, Semmelweis University, H-1094, Budapest, Hungary

[5]Institute of Plant Biology, Biological Research Centre, POB 521, H-6701, Szeged, Hungary

[6]Department of Plant Sciences, Wageningen University Research Centre, 6708 PB Wageningen, The Netherlands

[7]Laboratory of Proteomic Research, Biological Research Centre, POB 521, H-6701 Szeged, Hungary

[8]Technical Analytical Research Group of HAS, H-1111 Budapest, Hungary

[9]Co-senior authors

[#] These authors contributed equally to this work

*Correspondence: beatrix.horvath@rhul.ac.uk (B.M.H) and ben.scheres@wur.nl (B.S)

ABSTRACT

The rapidly proliferating cells in plant meristems must be protected from genome damage. Here we show that the regulatory role of the *Arabidopsis* RETINOBLASTOMA RELATED (RBR) in cell proliferation can be separated from a novel function in safeguarding genome integrity. Upon DNA damage, RBR and its binding partner E2FA are recruited to heterochromatic γH2AX- labelled DNA damage foci in an ATM and ATR-dependent manner. These γH2AX labelled DNA lesions are more dispersedly occupied by the conserved repair protein, AtBRCA1, which can also co-localise with RBR foci. RBR and AtBRCA1 physically interact *in vitro* and *in planta*. Genetic interaction between the RBR-silenced *amiRBR* and At*brca1* mutants suggests that RBR and AtBRCA1 may function together in maintaining genome integrity. Together with E2FA, RBR is directly involved in the transcriptional DNA damage response as well as in the cell death pathway that is independent of SOG1, the plant functional analogue of p53. Thus, plant homologs and analogues of major mammalian tumour suppressor proteins form a regulatory network that coordinates cell proliferation with cell and genome integrity.

RUNNING TITLE: Role of RBR, E2FA, AtBRCA1 in plant DDR

KEYWORDS: *Arabidopsis*/BRCA1/DNA damage response/E2FA/ RETINOBLASTOMA-RELATED

INTRODUCTION

The continuous post-embryonic growth of plants is supported by rapidly proliferating cells in meristems. Protection against the accumulation of mutations in dividing cells is not only important to maintain cellular functions, but additionally to maintain the source for generative cells throughout plant life (Hu *et al.*, 2015, Scheres, 2007). The *Arabidopsis* RETINOBLASTOMA RELATED (RBR) is a conserved regulator of cell proliferation, differentiation and stem cell niche maintenance (Harashima & Sugimoto, 2016). RBR regulates cell proliferation by restraining E2F dependent transcription of cell cycle genes (Gutzat *et al.*, 2012, Harashima & Sugimoto, 2016, Kobayashi *et al.*, 2015, Magyar *et al.*, 2005). Mitogenic signals promote RBR phosphorylation by Cyclin Dependent Kinases (CDKs) in association with D-type Cyclins, the best characterised being CYCLIN D3;1 (CYCD3;1) (Dewitte *et al.*, 2003, Magyar *et al.*, 2012). Upon this RBR phosphorylation, the E2FB transcription factor is released and promotes cell cycle gene expression and cell proliferation, while E2FA remains associated with phosphorylated RBR and maintains meristems through repression of differentiation (Harashima *et al.*, 2013, Kuwabara & Gruissem, 2014, Polyn *et al.*, 2015). The developmental role of RBR is best understood in the root meristem, where slowly dividing quiescent centre (QC) cells maintain surrounding root stem cells that divide more frequently. The low rate of cell division in the QC protects cells against DNA damage while surrounding stem cells are more sensitive (Fulcher & Sablowski, 2009, Furukawa *et al.*, 2010). RBR, in complex with the transcription factor SCARECROW, was shown to regulate specific stem cell divisions but also impose quiescence, which is important to protect against replication stress-induced cell death (Cruz-Ramirez *et al.*, 2012, Cruz-Ramirez *et al.*, 2013). RBR is also required during meiosis for chromosome condensation and synapsis of homologous

chromosomes, but not for introducing DSBs for homologous recombination (Chen *et al.*, 2011).

DNA damaging environmental factors, such as ionizing radiation, ultraviolet light, excess of metalloid elements (Br, Al) and internal damage generated spontaneously during DNA metabolism, can all impact on genome integrity (Hoeijmakers, 2009). To counteract the consequences of DNA lesions, organisms have evolved DNA damage response pathways (DDR). The recognition of DNA damage by sensor proteins initiates a network of molecular events that recruit the DNA repair machinery, regulate transcription, control cell-cycle progression, eliminate damaged cells by cell death and enter into terminal differentiation or senescence (Ciccia & Elledge, 2010, Cools & De Veylder, 2009, Hu *et al.*, 2015, Sherman *et al.*, 2011, Su, 2006).

Depending on whether DNA damage results in exposed single strand (SS) or double strand breaks (DSB), different signalling pathways are induced, involving alternative sets of sensors, mediators and effectors (Ciccia & Elledge, 2010). The central components are largely conserved among yeasts, animals and plants, although kingdom-specific proteins are also involved (Amiard *et al.*, 2013, Harper & Elledge, 2007, Waterworth *et al.*, 2011, Yoshiyama *et al.*, 2013b). The conserved DNA-damage sensing kinase ATAXIA-TELANGIECTASIA MUTATED (ATM) is activated by double strand DNA breaks (DSB) and acts during G1/S and G2/M checkpoints; its role recently was also implicated in the regulation of oxidative stress (Shiloh, 2014, Shiloh & Ziv, 2013). The ATAXIA-TELANGIECTASIA-AND-RAD3-RELATED (ATR) mainly responds to free single-stranded DNA, formed during processing of blocked replication forks, at G1/S and intra S checkpoints (Amiard *et al.*, 2013, Cimprich & Cortez, 2008, Culligan & Britt, 2008, Culligan *et al.*, 2006, Flynn & Zou, 2011).

In mammalian systems, the ATM kinase phosphorylates the histone variant H2AX (γH2AX) upon activation by DSB and initiates a cascade of events through recruiting numerous signalling proteins and DNA repair proteins, such as the breast and ovarian cancer type1 susceptibility protein, BRCA1. Single stranded DNA, the signal for replication stress, is sensed and bound by the mammalian replication protein A (RPA) to form a complex. The resulting complex activates ATR leading to the phosphorylation of the tumour suppressor protein, p53 and delay of S-phase, allowing the recovery of collapsed replication forks (Ciccia & Elledge, 2010).

No direct homologs of p53 have been identified in plants (Yoshiyama *et al.*, 2013b), but the plant-specific transcription factor, SUPPRESSOR OF GAMMA RESPONSE 1 (SOG1) is considered to be a functional analogue of p53 (Cimprich & Cortez, 2008, Yoshiyama *et al.*, 2013b). SOG1 is directly phosphorylated and activated by ATM. Active SOG1 induces transcription of genes related to DNA damage response and genes that impose cell-cycle checkpoint or repair (Culligan *et al.*, 2006, Ricaud *et al.*, 2007, Yoshiyama *et al.*, 2009). Upon DNA damage, ATM- and ATR activate the WEE1 kinase, which mainly controls the replication checkpoint (Cools *et al.*, 2011, De Schutter *et al.*, 2007, Dissmeyer *et al.*, 2009). The G2/M DNA damage checkpoint is controlled by the CDKA;1 inhibitors, SIAMESE-RELATED 5 and 7, direct targets of phosphorylated SOG1 upon DNA damage (Yi *et al.*, 2014).

Here we show that RBR, besides its well-known function during cell-cycle, maintains genome integrity in root meristematic cells. During DNA damage response, RBR together with E2FA accumulates at distinct heterochromatic foci labelled by γH2AX in an ATM/ATR dependent manner. AtBRCA1 is generally recruited to numerous γH2AX-labelled foci upon damage, but less frequently it also co-localizes with RBR. Co-immunoprecipitation and bimolecular fluorescence complementation (BiFC) studies show

that these two proteins can interact and genetic data support that they act together in protecting the genome. In addition, RBR/E2FA acts as a transcriptional repressor of AtBRCA1 transcription in parallel to the SOG1-governed transcription of DDR genes.

RESULTS

The role of RETINOBLASTOMA RELATED in mediating maintenance of genome integrity is separable from its function in cell-cycle regulation

Reduced RBR levels in the quiescent centre lead to extra cell divisions and sensitivity to genotoxic agents (Cruz-Ramirez *et al.*, 2013). To investigate whether the observed cell death was associated with S-phase progression, we quantified DNA synthesis using 5-Ethynyl-2´-deoxyuridine (EdU) incorporation and cell death in two Col-0 transgenic lines with reduced RBR levels; the *$35S_{pro}$:amiGORBR* (*amiRBR*) line, in which an artificial miRNA against RBR is expressed constitutively (Cruz-Ramirez *et al.*, 2013), and the *RCH1::RBR* RNAi (*rRBr*) line, in which an antisense RNA is expressed locally in the root meristem (Wildwater *et al.*, 2005). Both lines conferred similar phenotypes in the root with respect to extra stem cell divisions and increased S-phase labelling (Fig 1A and C for *amiRBR*; Fig EV1A and B for *rRBr*), which correlated with accumulating cell death both in the root tip of *amiRBR* (Fig 1B and D) and in *rRBr* (Fig EV1C).

To investigate whether cell death upon RBR silencing was due to a general deregulation of cell cycle entry, or reflected a specific role of RBR in cell viability, we analysed *CYCD3.1* overexpression, which promotes cell cycle progression through RBR phosphorylation (Dewitte *et al.*, 2003, Dewitte *et al.*, 2007, Magyar *et al.*, 2012, Nowack *et al.*, 2012) and *E2FA* and *E2FB* overexpression, which act downstream of RBR (De Veylder *et al.*, 2002, Magyar *et al.*, 2005, Magyar *et al.*, 2012). For proper comparison of accessions, the Ler line named G54, overexpressing *CYCD3.1* (Dewitte *et al.*, 2003, Riou-Khamlichi *et al.*, 1999) was introgressed into Col-0 (Appendix Supplementary Methods). The introgressed line showed increased EdU labelling and cell division

compared to Col-0 similar to *amiRBR* (Fig 1A and C). In contrast, no cell death was observed upon *CYCD3.1* overexpression (Fig 1B and D).

Similar to *CYCD3.1*, the overexpression of *E2FA-DPA* (De Veylder *et al.*, 2002)) or *E2FB-DPA* ((Magyar *et al.*, 2005) Appendix Supplementary Methods) in transgenic Col-0 lines led to extra cell divisions in the stem cell niche and EdU labelling compared to wild-type controls (Fig EV1D). However, the cell death response remained comparable to Col-0 (Fig EV1E). Our *CYCD3.1* and *E2F* overexpression results indicated that the cell death response is not the consequence of deregulated cell proliferation by the RBR pathway but specifically linked to reduced RBR levels.

Cell death upon RBR silencing might be a consequence of replication stress mediated DNA damage. To visualise DNA damage, we followed the accumulation of the phosphorylated H2AX (γH2AX) histone variant. As shown above, the extent of EdU incorporation was comparable between *amiRBR* and Col-0*(CYCD3.1OE)*, but the frequency of nuclei with γH2AX foci was around 4 times higher in *amiRBR* (~19%) and twice as much in Col-0*(CYCD3.1OE)* (~10%) compared to Col-0 (~5,5%; Fig 1E and F). Collectively, our data indicated that increased DNA damage upon reduction in RBR levels is separable from cell cycle regulation and associated with cell death.

Because RBR silencing led to spontaneous DNA damage and cell death, we tested whether the *amiRBR* line showed increased sensitivity to genotoxic stresses conferred by the DNA cross-linker mitomycin (MMC), double-strand break inducer zeocin, and replication stress inducer hydroxyurea (HU) (Hu *et al.*, 2015). Cell death responses in *rRBr* and *amiRBR* lines were stronger than in Col-0 upon MMC and zeocin treatments (Fig 2A-C), indicating that genotoxic stress-induced cell death response is suppressed by RBR. In contrast, HU treatment neither triggered cell death in Col-0 nor increased the

response in *amiRBR* (Fig 2D). In line with the cell death response, the number of γH2AX positive nuclei upon MMC treatment increased further in the *amiRBR* lines compared to Col0 (Fig 2E and F).

DNA stress recruits RBR to γH2AX-labelled heterochromatic foci

The role of RBR in maintaining genome stability and repressing genotoxic-stress-induced DNA damage might involve recruitment of RBR to DNA damage foci. Without genotoxic stress, RBR is diffusely localised within nuclei (Magyar *et al.*, 2012); and Fig 3A and C, Control). MMC treatment (16hrs) induced the accumulation of RBR in typically few large foci (1-5 foci per nucleus, Fig 3A and C, MMC). Around 17% of the examined nuclei contained RBR foci (total number of nuclei, N=845, biological repeat, n=3), mostly co-localised with γH2AX positive sites (Fig 3A). 3D reconstruction of serial sections revealed a partial co-localization of RBR and γH2AX foci with a broad correlation range, which is typical for dynamic and transient protein interactions (Fig 3B and E). A large proportion (80%; n=102) of the analysed RBR foci localized in close vicinity of heterochromatin, as confirmed by intensity profiles (Fig EV2A). The centromeric Histone 3 (CenH3) was also detected together with RBR foci upon MMC treatment (Fig EV2B).

Consistent with the localization of tobacco E2F in genotoxic-stress induced foci (Lang *et al.*, 2012), an E2FA fusion protein under its native promoter (Henriques *et al.*, 2010) significantly co-localised with RBR in foci after treatment with genotoxic agents (Fig 3C and E). To test whether RBR and E2FA localisation to these foci depends on DNA damage signalling, we used inhibitors KU55933 for ATM (IATM) and VE-821 for ATR (IATR), which revealed to be effective in plants by additively inhibiting the MMC-induced cell death response (Fig 3F). The simultaneous inhibition of the ATM and ATR kinases by these drugs also abolished both RBR and E2FA focus formation (Fig 3C, IATM and IATR

+MMC). In support of a role for both RBR and E2FA on DNA damage sites, RBR-E2FA foci partially co-localised at γH2AX positive sites (Fig 3F).

RBR silencing triggers AtBRCA1 recruitment to DNA damage foci and AtBRCA1 co-localises with RBR foci upon DNA stress

BRCA1 is a pivotal DNA repair protein of double strand DNA damage both in mammals (Rosen, 2013) and in *Arabidopsis* (Block-Schmidt *et al.*, 2011, Trapp *et al.*, 2011). *Atbrca1-1* (Reidt *et al.*, 2006) and *Atbrca1-3* loss of function mutants displayed a hypersensitive cell death response to genotoxic stress (MMC treatment) compared to Col-0 (Figs 4A and EV3A-C). We generated a genomic AtBRCA1-GFP construct driven by the endogenous promoter (AtBRCA1-GFP) (Appendix Supplementary Methods) and transformed it into the *Atbrca1-1* line. The AtBRCA1-GFP construct complemented the cell death response of the *Atbrca1-1* mutant (Figs 4A and EV3D and E). In untreated *Atbrca1-1*(AtBRCA1-GFP) root meristems, the GFP signal was low and diffuse in the nucleus, while the signal increased upon MMC treatment and accumulated in pronounced speckles of an increasing number of meristematic nuclei (Fig 4A) *Atbrca1-1*(AtBRCA1-GFP). Upon root-meristem specific silencing of RBR in the *rRBr* line, AtBRCA1-GFP also accumulated in nuclear speckles in and around the stem cell niche area indicating that the localization of AtBRCA1 is induced by RBR reduction and is not critically dependent on RBR (Fig 4B).

AtBRCA1-GFP nuclear speckles co-localised with γH2AX foci, after MMC treatment (Fig 4C) and thus we investigated whether RBR is co-recruited with AtBRCA1 at γH2AX foci by triple immuno-co-localisations of RBR, AtBRCA1-GFP and γH2AX in the *Atbrca1-1*(BRCA1-GFP) line (Fig 4C). Similar proportions of γH2AX positive nuclei showed co-localisation of γH2AX foci either with AtBRCA1-GFP or RBR (25% and 27%,

respectively; Table 1). The AtBRCA1 and γH2AX overlapping foci were small and numerous in most nuclei and well distinguishable from the large and sparse RBR-γH2AX co-labelled foci. The two different classes of foci rarely coexisted within the same cell (Fig 4C, Table 1). Foci with RBR and AtBRCA1 together at γH2AX sites appeared at lower frequency (10% of the $\gamma H2AX^{+}$ nuclei, N=452, n=3; Table 1) and their appearance resembled the large RBR-γH2AX foci. RBR and AtBRCA1 co-localised only in the presence of γH2AX. When ATM and ATR kinase inhibitors were applied simultaneously with MMC, these inhibitors reduced the number of nuclei with γH2AX and AtBRCA1-GFP foci and abolished the formation of RBR foci (Fig 3C).

To test whether RBR can be recruited to γH2AX foci in the absence of AtBRCA1, we monitored RBR and γH2AX foci upon MMC treatment in the *Atbrca1-1* mutant. We observed co-localisation of RBR and γH2AX in large and sparse foci as in the control, suggesting that RBR recruitment is independent of AtBRCA1 (Fig 4D).

To study whether AtBRCA1 and RBR proteins might physically interact, we translated both proteins *in vitro* in wheat germ extract and performed co-immuno-precipitations (Appendix Supplementary Methods). RBR specifically interacted with AtBRCA1, but was weaker than the positive control, E2FA (Fig 5A). The observed direct interaction between RBR and AtBRCA1 was confirmed by bimolecular fluorescence complementation (BiFC) assays in young, growing tobacco leaves in the presence or absence of MMC. RBR-SCARECROW complex formation (Cruz-Ramirez *et al.*, 2012) served as positive control and AtBRCA1-SCARECROW interaction as negative control. RBR and SCARECROW formed a complex within 36 h after infiltration, while RBR and AtBRCA1 complex formation could be detected after 48h in the nucleus. In rare cases the interaction was observed in foci (Fig 5B). These data indicated that RBR and AtBRCA1 are independently recruited to DNA damage foci but have the ability to interact.

RBR and At*BRCA1* genetic interaction suggests common roles in maintaining genome integrity

To study whether RBR and AtBRCA1 might function together, we studied their genetic interaction. Based on genotyping and segregation analysis of linked resistance markers, the *amiRBR;Atbrca1-1* cross was homozygous for both loci, yet around half of the seedlings showed strong developmental abnormalities, such as mis-positioned or missing organs or seedling lethality (Fig EV4A and B), indicating a variably penetrant window of sensitivity for the lack of AtBRCA1 and compromised RBR level during embryogenesis. The *amiRBR;Atbrca1-1* seedlings that looked largely normal displayed extra stem cell divisions and increased S-phase entry in the root meristem, both phenotypic confirmations for the effective RBR silencing (Fig EV4D-G), and the *AtBRCA1* expression could not be induced in the introgressed line confirming the presence of the mutant *AtBRCA1-1* allele (Fig EV4C). The frequency of γH2AX positive nuclei in the *Atbrca1-1* and *amiRBR* parents and the *amiRBR;Atbrca1-1* cross were similar (Fig 6A and B), which is consistent with a scenario where RBR and AtBRCA1 act together in a common pathway to maintain genome integrity.

We also studied whether AtBRCA1 function may be required for the cell death response observed in the *amiRBR*, and found that both in the *amiRBR,Atbrca1-1* and *amiRBR;Atbrca1-3* crosses the cell death was substantially suppressed (Fig 6C), as quantified in the distal stem cell niche (Fig 6D). The lack of AtBRCA1 function had no substantial influence on other RBR-regulated processes such as columella stem cell division or S-phase entry (Fig EV4D-G).

To test whether BRCA1 expression is sufficient to induce cell death, we expressed a *myc* tagged genomic *AtBRCA1* fusion under the control of the GVX β-

estradiol-inducible promoter (*GVX1090$_{pro}$:AtBRCA1$_{gen}$:10xmyc*) in the *Atbrca1-1* mutant. After 24h of induction, no cell death developed, indicating that elevation of BRCA1 transcription cannot trigger cell death on its own (Appendix Fig S1 and Supplementary Methods). These observations indicate that AtBRCA1 is required but not sufficient to trigger a cell death response when RBR cannot maintain genome integrity.

RBR regulates DDR gene transcription through E2FA

The observed recruitment of RBR together with E2FA as a complex at DNA lesions might start the signalling process for the transcriptional regulation of DNA damage response genes. To investigate transcriptional responses to RBR down-regulation in the root tip, we performed genome-wide transcriptome profiling of the meristematic region (representative root-tips of each time point are shown in Fig EV1A) in three independent biological replicates (Appendix Supplementary Methods). We identified 99 differentially expressed genes between *rRBr* and Col-0 root tips, of which 82 genes were up- and 17, including *RBR,* were down-regulated (Appendix Table S1). Gene ontology (GO) analysis revealed significant enrichment for genes encoding nuclear proteins functionally related to three major processes: (1) nucleosome - and chromosome assembly and maintenance; (2) replication and cell cycle checkpoint control; (3) DNA damage response and repair (Fig 7A, Appendix Table S1 and Appendix Supplementary Methods). The transcriptional changes in a set of genes representing different functional and co-expressional categories (Appendix Table S2 and Fig S2 and Supplementary Methods) were confirmed by qRT-PCR both in *rRBr* root-tips, where *RBR* is silenced in root meristems (Fig 7B and C), and in seedlings from *amiRBR* where post-embryonic RBR levels are reduced constitutively using the *35S* promoter (Fig 7D). The transcriptional changes were comparable in *rRBr* and *amiRBR* lines and in full agreement with the

microarray data. Importantly, *AtBRCA1* was among the DDR targets that were up-regulated upon RBR silencing.

The presence of canonical E2F binding sites in the 1kb-promoter region of the differentially expressed genes (53 out of 99, summarised in Table S1 column N, based on (Naouar *et al.*, 2009) suggested that RBR exerts its repressive activity through E2F proteins. Chromatin Immuno-Precipitation (ChIP) assays were carried out on root tissues using RBR specific antibody (Horvath *et al.*, 2006) in three independent biological repeats followed by qRT-PCR on the promoter of the *AtBRCA1* (Fig 7F). Significant enrichment of RBR was detected on distinct regions of the *AtBRCA1* promoter. The enrichment on fragment 2 that contained two putative E2F binding motifs (Fig 7E; -234^{+}:ggggcaa and -151^{-}:tttggcgc), exceeded the enrichment detected on the *PCNA1* promoter used as a positive control (Fig 7F). A reduced level of enrichment (+/-3 times) was also observed in neighbouring regions lacking putative binding sites, which may be attributed either to the heterogeneous size of sonicated fragments (+/-300-500bp) or to E2F binding to non-consensus sequences.

To address which of the activator E2Fs might partner with RBR to regulate DDR gene expression, we quantified transcription of *AtBRCA1* in *e2fa-1*, *e2fa-2*, *e2fb-1* (MPIZ_244, GABI-348E09, SALK_103138, respectively; (Berckmans *et al.*, 2011b) and *e2fb-2* (SALK_120959) mutants. Similar to *amiRBR, AtBRCA1* expression increased in *e2fa-1* but not in *e2fa-2* mutants nor in any of the *e2fb* mutants when compared to Col-0 (Fig 8A). The difference in the *AtBRCA1* expression in the two *e2fa* lines likely relates to the different sites of insertion in the two alleles. Both *e2fa* mutant alleles are predicted to encode a truncated E2FA proteins that lack the transactivation and the canonical RBR binding domains, but retain the DNA-binding and dimerization domains. In contrast to *e2fa-2*, the *e2fa-1* allele also lost the putative 'marked box' domain (Fig EV5A), which

was described in mammalian E2Fs to provide a second interaction interface with Rb's C-terminal domain (Dick & Rubin, 2013, Ianari *et al.*, 2009). *AtBRCA1* de-repression in *amiRBR;e2fa-1* and *amiRBR;e2fa-2* double homozygous lines did not exceed the de-repression seen in *amiRBR*, further validating that RBR represses *AtBRCA1* through the DNA-binding E2FA transcription factor (Fig 8A). The level of RBR silencing in the double mutants is shown in Fig EV5B. Among the RBR-repressed DDR related genes tested, only *SMR4* was similarly regulated as *AtBRCA1* by RBR and E2FA (Fig EV5E). Interestingly, MMC-induced *AtBRCA1* expression was suppressed in *e2fa-1* but not in *e2fb* mutants (Fig 8B), suggesting that E2FA is specifically required for genotoxic stress induced *AtBRCA1* expression.

RBR represses E2FA activity to inhibit cell death response

To test whether E2FA can directly bind to the *AtBRCA1* promoter we performed ChIP analysis using $AtE2FA_{pro}$*:*$AtE2FA_{gen}$*:GFP* seedlings and $35S_{pro}$*:GFP* controls (Magyar *et al.*, 2012). E2FA-GFP was highly enriched on the segment of the *AtBRCA1* promoter containing two putative E2F binding sites (Fig 8C) and the enrichment was reduced when seedlings were treated with MMC (Fig 8C), indicating that, upon genotoxic stress, RBR-E2FA mediated repression of *AtBRCA1* is released. To investigate whether the release may rely on a change in E2FA-RBR interaction upon genotoxic stress, we pulled down the complex through the E2FA-GFP and quantified known complex components by label free mass spectrometry. We found that the association of RBR with E2FA and the DPs became stronger upon MMC treatment as indicated by the ratio of the quantified MS spectra of the complex components (Appendix Table S4). Interestingly, in the E2FA-GFP pull downs we could never detect any of the components of the multi-protein DREAM complex, (*D*P, *R*B-like *E*2F, *a*nd *M*uvB, Sadasivam & DeCaprio, 2013), while with E2FB-GFP, these proteins were readily pulled down (Appendix Table S5). This may suggest

that E2FA functions in different complex(es) than the DREAM associated with E2FB and E2FC (Kobayashi *et al.*, 2015).

As RBR repression acts through E2FA to regulate transcription of at least two DDR genes, we investigated whether this regulation functions also in the cell death response. We quantified cell death in the two *e2fa* mutant lines alone and in combination with *amiRBR*. Neither *e2fa-1* nor *e2fa-2* showed any cell death response, and root development was also normal. Importantly, spontaneous cell death in *amiRBR* was completely suppressed in the *amiRBR;e2fa-1* and strongly delayed and reduced in the *amiRBR;e2fa-2* crosses (Fig 8D) while RBR silencing remained effective (Fig EV5B), demonstrating that the RBR silencing-induced cell death response is dependent on E2FA function. To test whether E2FA is also required for genotoxic stress-induced cell death, we treated *e2fa* mutants with MMC. Cell death upon genotoxic stress was partially suppressed in *e2fa-1* and *e2fa-3* (Xiong *et al.*, 2013) lines, but not by *e2fa-2* (Figs 8E and quantified in EV5C and D), confirming that the cell death is generally dependent on E2FA and is mediated through the marked box.

E2FA and RBR are required for genotoxic stress-induced DDR in a SOG1 independent pathway

SOG1 is a pivotal transcription factor for the induction of DDR genes upon genotoxic stress. We observed significant overlap between DNA repair genes regulated by RBR (Appendix Table S1 column B) and genes with compromised induction by irradiation in the *sog1-1* mutant ((Appendix Table S1 columns B and L, respectively; ratio: 8/10). The *sog1-1* mutation can fully suppress cell death response upon genotoxic stress (Yoshiyama *et al.*, 2009, Yoshiyama *et al.*, 2013a). Based on this comparison, we asked whether the activation of the DNA damage response pathway upon RBR silencing is dependent on

SOG1 function. Homozygous *sog1-1* plants (Preuss & Britt, 2003) were transformed with the *35S$_{pro}$:amiGORBR* construct (Cruz-Ramirez *et al.*, 2013), and RBR silencing was confirmed in the *amiRBR*,*sog1-1* line (Fig EV6C). The cell death response in the *amiRBR*,*sog1-1* root meristem was comparable to the *amiRBR* line (Fig 9A and B), demonstrating that cell death induced upon RBR silencing is independent of SOG1. In the *amiRBR*,*sog1-1* lines, RBR silencing was effective (Fig EV6C) and transcription of all the tested DDR genes also remained elevated as in *amiRBR* (Fig 9C), showing that the release of RBR-mediated transcriptional repression is also SOG1 independent. As expected, the genotoxic stress-induced DDR gene expression (Fig 9D) and cell death response by MMC (Fig EV6A and D) and zeocin (Fig EV6B) treatments were fully suppressed in the *sog1-1* plants, but not in the *amiRBR*,*sog1-1* lines, further confirming that RBR acts on a SOG1 independent pathway. HU does not activate SOG1 to induce DDR (Yoshiyama *et al.*, 2013a), and hence accordingly did not have any effect in the *amiRBR* and *amiRBR*,*sog1-1* lines (Fig EV6B). Taken together, RBR regulates DDR gene transcription and cell death at least in part through a SOG1-independent pathway.

DISCUSSION

Here we show that the plant Retinoblastoma homologue, RBR, has a direct role in maintaining genome integrity. RBR is recruited to a limited number of large heterochromatic DNA damage foci together with E2FA in an ATM- and ATR-dependent manner upon DNA damage. AtBRCA1 and RBR are independently recruited to these specific damage foci, they interact and our genetic study show that they partially act together to maintain genome integrity and to prevent cell death. The accompanying paper of Biedermann et al. shows that RBR is required to localize RAD51 and that RBR and RAD51 co-localize in these large foci, corroborating a non-transcriptional role for RBR in the maintenance of plant genome integrity. We further show that RBR and E2FA also

have transcriptional DNA damage response roles that act in parallel to the well-established SOG1 pathway. Below we discuss how this evidence for a possible dual cell cycle-independent role of RBR in the meristematic DNA damage response at γH2AX foci and at target gene promoters fits in with recent evidence from plant and mammalian experimental systems.

RBR mediated DNA damage control at γH2AX foci

When mammalian Rb proteins are deregulated, aberrant S-phase progression can result in nucleotide pool deficiency, replication fork stalling and DNA damage (Bester *et al.*, 2011). Even with haploid wild-type Rb, mammalian cells show chromosome defects and aneuploidy (Coschi *et al.*, 2014, Hinds, 2014). Similarly, in plants, reduction of RBR function in the *rbr-3* mutant (Johnston *et al.*, 2010) and in transgenic plants overexpressing the viral RepA protein inactivating RBR (Henriques *et al.*, 2010) resulted in aneuploidy. Our data corroborate that, in plants, S phase progression due to RBR deregulation can contribute to DNA damage but we show that this effect is separable from a direct role of RBR in DNA damage control.

Our finding that DNA damage induces ATM/ATR dependent recruitment of RBR and E2FA to γH2AX foci suggests a direct, non-transcriptional role for RBR in DNA damage control. The reported accumulation of *Nt*E2F in γH2AX labelled foci at the G1/S transition in tobacco cells is consistent with this notion (Lang *et al.*, 2012). Also, consistent with non-transcriptional roles for RBR is the finding that, during meiosis, RBR is recruited to chromosomes in a DNA DSB-dependent manner, where it was suggested to facilitate the assembly of chromatin modifiers, repair proteins and condensin complexes for homologous recombination through their LxCxE motifs (Chen *et al.*, 2011).

In mammals, Rb localizes to chromatin at S-phase after DNA damage (Avni *et al.*, 2003). Furthermore, E2F1 (Coschi *et al.*, 2014) and E2F7 (Zalmas *et al.*, 2013) have transcription-independent roles to bring protein complexes to damaged DNA. E2F1 and Condensin II are recruited by pRb to the pericentromeric region of the chromosome and to replication origins, thus facilitating correct replication, accurate chromosome condensation, and chromosome segregation (Coschi *et al.*, 2014, Hinds, 2014). Rb heterozygosity leads to loss of E2F1 and Condensin II binding, accompanied by replication stress labelled by increased γH2AX foci. Recently it was shown that Rb localizes to DSBs dependent on E2F1 and ATM to promote DSB repair through homologous recombination (Velez-Cruz *et al.*, 2016). We show that a similar mechanism might be operate in plants, where RBR localisation to DSBs requires ATM and ATR activities. Further similarities to the animal scenario are that, homogenously distributed tobacco E2F partly re-localises upon genotoxic stress and forms 2-3 foci per nucleus in BY-2 tobacco cells. For these focus formation, the transactivation domain and the RBR binding site were shown to be critical. Also, the plant Condensin complex II appears to play a role in alleviating DNA damage by HR or compacting the genome in response to genomic stress (Sakamoto *et al.*, 2011). It will be interesting to investigate in the future whether a similar non-transcriptional role for RBR, E2FA and Condensin II complexes in genome integrity is also operational in plants.

In mammalian cells, Rb interacts with HsBRCA1, which was suggested to be important to repress cell proliferation (Aprelikova *et al.*, 1999). In *Arabidopsis,* we did not detect any cell proliferation effect either after induced AtBRCA1 overexpression or in the *Atbrca1* mutants. In human cells, Rb was also shown to recruit HsBRCA1 in order to facilitate processing and repair of topoisomerase II induced DSB (Xiao & Goodrich, 2005). Recently, Rb was also shown to be directly involved in DSB repair, independently

of its cell-cycle function, through its interaction with components of the canonical non-homologous end-joining repair pathway (Cook *et al.*, 2015). It will be interesting to investigate the mechanism of RBR and AtBRCA1 interaction at these specific heterochromatic sites with damaged DNA, and what their joint function is in DNA damage control in *Arabidopsis*.

RBR mediated transcriptional responses to DNA damage

Cells with excessive damage are eliminated. The coordination of cell proliferation and apoptosis in mammalian cells relies on the formation of the Rb-E2F1 complex by interaction of Rb's carboxy-terminal domain and the marked box of E2F1 (Carnevale *et al.*, 2012, Dick & Rubin, 2013). During S-phase, the phosphorylated Rb-E2F1 complex represses pro-apoptotic genes, while in response to DNA damage upon ATM-dependent phosphorylation of E2F1, this complex becomes a transcriptional repressor on the cell cycle genes and activator on the pro-apoptotic genes (Dick & Rubin, 2013, Ianari *et al.*, 2009). There are indications that a similar mechanism may function in *Arabidopsis*. RBR forms a complex with E2FA, which remains stable upon CYCD3;1-CDKA phosphorylation during the cell cycle (Magyar *et al.*, 2012). In animal cells, phosphorylation of Rb by CycD:Cdk4/6 kinases diversifies rather than merely inactivates Rb complexes (Narasimha *et al.*, 2014). RBR phosphorylation upon CYCD3.1 overexpression in plants might similarly lead to the formation of distinct regulatory complexes with roles in activation of G1 to S transition and roles protecting against cell death or differentiation. In agreement, we find that silencing of RBR leads to a very different outcome than RBR phosphorylation. It initiates cell death response fully relying on E2FA with an intact "marked box" domain, suggesting a conserved mechanism between kingdoms. Importantly, not all the RBR-repressed DDR genes are E2FA regulated. AtBRCA1 is an essential target, as its function was required but not sufficient to induce cell death upon

transcriptional de-repression. As cell death response was fully suppressed in *e2fa-1*, in relation to AtBRCA1, additional genes should be involved in the induction of cell death process. Interestingly, both AtBRCA1 and E2F functions are required also for the pathogen-induced cell death during hypersensitive response in plant defence (Bao & Hua, 2015, Zebell & Dong, 2015)

Active SOG1 is the pivotal transcription factor in plant DDR upon genotoxic stress (Yoshiyama *et al.*, 2013b). Here we show that E2FA also carries out this function, since MMC-induced activation of DDR genes, such as *AtBRCA1* and *SMR4,* is compromised both in *sog1-1* and *e2fa-1* mutants. The ability of E2FA to activate DDR genes is dependent on RBR levels or activity, which are responsive to intrinsic cell cycle-dependant and cell extrinsic signals in a SOG1 independent pathway.

In conclusion, RBR, mainly known as a regulator of cell cycle and asymmetric cell division in plant meristems, is also involved in maintaining genome integrity in these growth zones through two functions, (i) assembly at a limited number of H2AX foci together with E2F and, possibly, AtBRCA1; (ii) transcriptional regulation of important DDR genes including *AtBRCA1*. It will be interesting to investigate in the future whether and how assembly of E2F-RBR complexes at particular γH2AX foci is coupled to the transcriptional role of these complexes in DDR gene regulation.

MATERIALS AND METHODS

Plant material and growth conditions

Seeds were sterilised and grown as described earlier (Wildwater *et al.*, 2005) except that seedlings used for microarray analysis and qRT-PCR were germinated on 1,2 % plant agar. *Arabidopsis* thaliana ecotype Columbia 0 (Col-0) was used as wild type; T-DNA insertion lines, *Atbrca1-3* (SALK_099751) and *e2fb-2* (SALK_120959) were obtained from the Nottingham *Arabidopsis* Stock Centre. The transgenic lines, *sog1-1* (Yoshiyama *et al.*, 2009), *e2fa-1, e2fa-2* and *e2fb-1* (MPIZ_244, GABI-348E09, SALK_103138, respectively,(Berckmans *et al.*, 2011b), (Berckmans *et al.*, 2011a)*, e2fa-3* (Xiong *et al.*, 2013), At*brca1-1* (Reidt *et al.*, 2006), *rRBr* (Wildwater *et al.*, 2005) and *amiRBR* (Cruz-Ramirez *et al.*, 2012) were described earlier. The T-DNA insertions, mutations were confirmed by PCR based genotyping or sequencing and gene silencing was demonstrated via gene expressional studies and phenotyping. To study the *amiRBR;sog1-1* phenotype, more than 20 independent transformants were generated, genotyped by sequencing the *sog1-1* locus and analysed for *RBR* silencing. The overexpression lines *E2FA-DPA* (De Veylder *et al.*, 2002)) and *CYCD3.1OE* (Dewitte *et al.*, 2003, Riou-Khamlichi *et al.*, 1999) were described earlier. The construction of *E2FB-DPA* (Magyar *et al.*, 2005) is described in the Appendix Supplemantary Methods.

Chemical treatments and induction studies

To induce DNA damage response, 5-6 day-old seedlings, were transferred to tissue culture plates (unless stated otherwise), containing fresh MS liquid medium without or with 10 µg/ml mitomycin C (MMC), 20 or 3 µg/ml zeocin or 1 mM hydroxyurea (HU) and

treated for 16 h or alternatively for short treatment periods of 1-4 h. For kinase inhibitory assay, 5-6 day old seedlings were pre-incubated for 2 h in ATM or ATR kinase inhibitors (Selleckchem, KU55933, VE-821, respectively) which was applied to the MS liquid medium at 10 μM final concentration, afterwards MMC was given, as described above. Appropriate controls and mutants, were treated simultaneously and all treatments were repeated at least three times (n=biological repeat) with 15-20 (N=sample size) replicates. Although the level of MMC induction was varied between the different experiments, the ratio between controls and treated samples were comparable. Cell death in root tips was quantified by counting the number of PI-stained cells in the columella stem cells (CSC) and lateral root cap initials (LRC) and their daughter cells, and by measuring the contiguously PI-stained cell area directly adjacent to the QC in the proximal meristematic vasculature

Immuno-fluorescence labelling and fluorescence microscopy

Root excision and slide preparation of squashed root-tips and immuno-labelling with *Arabidopsis* anti-γH2AX and others was performed according to (Amiard *et al.*, 2010, Friesner *et al.*, 2005) with slight modifications; 3.7% paraformaldehyde with 0.05 % Triton was used for 1hr and enzyme treatment was applied on root-tips transferred and attached to microscopic slides. For dilution of primary and secondary antibodies see Supplementary Information. 5-Ethynyl-2´-deoxyuridine (EdU) labelling was performed in whole mount preparation of root tips, details see also in Supplementary Methods.

For fluorescence microscopy Olympus IX-81 FV-1000 confocal imaging system was used. For details of confocal laser scanning microscopy, image acquisition and processing see Appendix Supplementary Methods. For Imaris section, z-stacks were taken with 0.2 μm z-step. Images were de-convolved using Huygens (Scientific Volume

Imaging, Hilversum, The Netherlands) to remove out-of-focus information and sectioning of gained 3D objects was performed using Imaris software (Bitplane) in the section mode. The quantitative co-localisation analysis was performed using ImageJ software with JACoP (Just Another Co-localisation Plug-in, (Bolte & Cordelieres, 2006) based on Pearson's coefficient. A Region of Interest was defined by a square of unified pixel size (26 x 26) and image correlation analysis was performed by combining single stacks of green and red fluorescent images. The data analysis was generated using the Real Statistics Resource Pack software (Charles Zaiontz; www.real-statistics.com).

For phenotypic analysis roots were stained in 5 µg/ml propidium-iodide (PI) and analysed on Leica SP2 or Olympus IX81-FV1000 inverted laser-scanning microscope. For qualitative and quantitative comparison, images were recorded with identical microscope settings in all cases. EdU staining of replicating cells was performed using Click-iT EdU Alexa Fluor 488 HCS Assay (Molecular Probes, Eugene, OR, USA) as described earlier (Vanstraelen *et al.*, 2009).

Bimolecular Fluorescent Complementation and transient transfection assay

For BiFC, AtBRCA1 cDNA was sub-cloned to pGEMT-easy 221 (see primers Appendix Table S3). Sub-cloning of SCR and RBR cDNAs were described earlier (Welch *et al.*, 2007), (Cruz-Ramirez *et al.*, 2012) respectively). To generate split YFP construct the binary BiFC GATEWAY-Destination vectors were used (Gehl *et al.*, 2009). Four-week-old *Nicotiana benthamiana* plants were infiltrated by *Agrobacterium tumefaciens* containing different constructs as described by (Liu *et al.*, 2010). The infiltrated region of the leaf was then mounted in water and checked for expression. YFP fluorescence was visualized using a Zeiss LSM 710confocal laser scanning microscope, and images were processed with the confocal microscope Zeiss ZEN software. Results from at least three

independent experiments and more than 20 infiltrated leaves were visualized.

Transcriptional profiling, expressional studies and cloning

A detailed description is provided in Appendix Supplementary Information. The micro-array data are submitted to GEO; the approval of the submission can be followed by the series entry: GSE47715.

Link: http://www.ncbi.nlm.nih.gov/geo/query/acc.cgi?acc=GSE47715.

Chromatin-Immuno Precipitation (ChIP)

ChIP was carried out on root material of 5 days-old Col-0 seedlings to study RBR enrichment and on Col-0(*E2FA$_{pro}$:E2FA$_{gen}$:GFP*) (Magyar *et al.*, 2012) seedlings without and with 16 h MMC treatment to analyse E2FA-GFP enrichment. Here, *35S$_{pro}$:GFP* was used as a control. To determine RBR enrichment, IP was performed in the absence and presence of antibody specific for RBR protein as described by Horvath et al. (2006). For the detection of E2FA-GFP, GFP-trap beads (Chromotek) were used as described earlier (Schepers *et al.*, 2001).

Primers for quantitative RT/PCR were designed to amplify fragments between 100 to 200 bps spanning the putative promoter region of *AtBRCA1*. The negative and positive controls are described earlier (Cruz-Ramirez *et al.*, 2012). Primer pairs were analysed on the same biological material, repeated three times with three technical replicates for RBR and twice for E2FA. Enrichment for RBR was calculated by comparing the PCR data derived from immuno-precipitation samples with and without antibody and for E2FA between Col-0(*E2FA$_{pro}$:E2FA$_{gen}$:GFP*) and *35S$_{pro}$:GF*P lines. Student's *t* tests were

performed to analyse statistical significance. List of primers is given in Appendix Table S3.

In vitro translation and pull-down

Full-length cDNAs for AtBRCA1 and RBR were obtained from the RIKEN Plant Science Centre and re-cloned into the pEU3II-HLICNot vector by ligation independent cloning. *In vitro* transcription, cell-free translation, pull-down and immuno-blotting were performed as described earlier (Nagy *et al.*, 2015). See also Appendix Supplementary Methods.

ACKNOWLEDGEMENTS

We thank Charles White, Simon Amiard (Clermont Université, France), Oliver Trapp, Holger Puchta (Institute of Technology, Karlsruhe, Germany), Alfredo Cruz-Ramirez (Laboratorio Nacional de Genomica para la Biodiversidad, Cinvestav Sede Irapuato, Mexico), Ann Britt (University of California, at Davis, USA), Jim Murray, Walter Dewitte (Cardiff School of Biosciences, Cardiff University, Wales, UK), Wenkun Zhou (Wageningen University, The Netherlands) for sharing material; Christian Bachem (Wageningen University, The Netherlands) and Arp Schnittger (Hamburg University, Germany) for critically reading the manuscript; Laszlo Bako and Pal Miskolci (Umeå University, Sweden) for technical advice in ChIP technology, Kinga Bachem (Wageningen University, The Netherlands) for illustration and Milian Bachem (University of Rotterdam, The Netherlands) for statistical analysis.

AUTHORS CONTRIBUTION

The authors have made the following declarations about their contributions:

B.M.H and B.S conceived the idea of analysing RBR targets and regulation of cell death, B.M.H, Z.M. and L.B. the links to E2Fs, B.M.H link to *sog1-1*. B.M.H. performed expressional studies, transcriptome analysis, generation and characterisation of mutants ChiP with RBR on *AtBRCA1* promoter; the immune-localisation and microscopical studies on localisation of RBR, E2FA, γH2AX and AtBRCA1 were performed by H.K and P.B., the expressional and phenotypic studies by E.N., experiments on RBR and AtBRCA1 binding in wheat-germ system by Sz.N. and T.M. and using BiFC technique by I.B, the analysis of the microarray data by B.M.H and G.S-P. Z.A. performed the cell death experiments with CYCD3;1oe line. ChIP analysis with E2FA-GFP protein was carried out

by Cs.P. and S.P. generated and analysed the *amiRBR,e2fa* mutant. Protein complex isolation, LC-MS/MS identification were performed by A.P-Sz. Zs.D**.** The manuscript was written by B.M.H., L.B, P.B. and B.S; seen and commented by all authors.

FUNDING

B.M.H was funded by a Marie-Curie IEF fellowship (FP7-PEOPLE-2012-IEF- 330789), and by the Netherlands Organization for Scientific Research, Spinoza grant to **B.S. G.S-P**. was funded by the Utrecht University Focus & Mass grant and CBSG2/NCSB. **Cs.P**. was funded by a Marie-Curie IEF fellowship (FP7-PEOPLE-2012-IEF 330713) and both, **Cs.P** and **L.B**. by the BBSRC-NSF grant (BB/M025047/1). **P.B.** was founded by Grant Agency of the Czech Republic 15-11657S P501. **Z.M**. and **E.N.** were funded by the Hungarian Academy, OTKA 107838 and with Campus Hungary, TÁMOP-4.2.4B/2-11/1-2012-0001 fellowship, respectively. **A.P-Sz.** was funded by János Bolyai Research Scholarship of the Hungarian Academy of Sciences. **S.P.** was funded by ERA-CAPS grant 2013/15548/ALW. The funders had no role in the design of the study, data collection and analysis, decision to publish, or preparation of the manuscript.

CONFLICT OF INTEREST

The authors declare that they have no conflict of interest.

ABBREVIATIONS

ATM: ATAXIA-TELANGIECTASIA MUTATED; ATR: ATAXIA-TELANGIECTASIA-AND-RAD3 RELATED; AtBRCA1: BREAST CANCER SUSCEPTIBILITY1; SOG1: SUPPRESSOR OF GAMMA IRRADIATION, GFP: GREEN FLUORESCENCE PROTEIN,

RBR: RETINOBLASTOMA-RELATED protein; γH2AX: HISTONE 2A, EdU: 5-Ethynyl-2´-deoxyuridine, GO: gene ontology; HR: homologous recombination; MMC: mitomycin C

REFERENCES

Amiard S, Charbonnel C, Allain E, Depeiges A, White CI, Gallego ME (2010) Distinct roles of the ATR kinase and the Mre11-Rad50-Nbs1 complex in the maintenance of chromosomal stability in Arabidopsis. Plant Cell 22: 3020-33

Amiard S, Gallego ME, White CI (2013) Signaling of double strand breaks and deprotected telomeres in Arabidopsis. Front Plant Sci 4: 405

Aprelikova ON, Fang BS, Meissner EG, Cotter S, Campbell M, Kuthiala A, Bessho M, Jensen RA, Liu ET (1999) BRCA1-associated growth arrest is RB-dependent. Proc Natl Acad Sci U S A 96: 11866-71

Avni D, Yang H, Martelli F, Hofmann F, ElShamy WM, Ganesan S, Scully R, Livingston DM (2003) Active localization of the retinoblastoma protein in chromatin and its response to S phase DNA damage. Mol Cell 12: 735-46

Bao Z, Hua J (2015) Linking the Cell Cycle with Innate Immunity in Arabidopsis. Mol Plant 8: 980-2

Berckmans B, Lammens T, Van Den Daele H, Magyar Z, Bogre L, De Veylder L (2011a) Light-dependent regulation of DEL1 is determined by the antagonistic action of E2Fb and E2Fc. Plant Physiol 157: 1440-51

Berckmans B, Vassileva V, Schmid SP, Maes S, Parizot B, Naramoto S, Magyar Z, Alvim Kamei CL, Koncz C, Bogre L, Persiau G, De Jaeger G, Friml J, Simon R, Beeckman T, De Veylder L (2011b) Auxin-dependent cell cycle reactivation through transcriptional regulation of Arabidopsis E2Fa by lateral organ boundary proteins. Plant Cell 23: 3671-83

Bester AC, Roniger M, Oren YS, Im MM, Sarni D, Chaoat M, Bensimon A, Zamir G, Shewach DS, Kerem B (2011) Nucleotide deficiency promotes genomic instability in early stages of cancer development. Cell 145: 435-46

Block-Schmidt AS, Dukowic-Schulze S, Wanieck K, Reidt W, Puchta H (2011) BRCC36A is epistatic to BRCA1 in DNA crosslink repair and homologous recombination in Arabidopsis thaliana. Nucleic Acids Res 39: 146-54

Bolte S, Cordelieres FP (2006) A guided tour into subcellular colocalization analysis in light microscopy. J Microsc 224: 213-32

Carnevale J, Palander O, Seifried LA, Dick FA (2012) DNA damage signals through differentially modified E2F1 molecules to induce apoptosis. Mol Cell Biol 32: 900-12

Chen Z, Higgins JD, Hui JT, Li J, Franklin FC, Berger F (2011) Retinoblastoma protein is essential for early meiotic events in Arabidopsis. EMBO J 30: 744-55

Ciccia A, Elledge SJ (2010) The DNA damage response: making it safe to play with knives. Mol Cell 40: 179-204

Cimprich KA, Cortez D (2008) ATR: an essential regulator of genome integrity. Nat Rev Mol Cell Biol 9: 616-27

Cook R, Zoumpoulidou G, Luczynski MT, Rieger S, Moquet J, Spanswick VJ, Hartley JA, Rothkamm K, Huang PH, Mittnacht S (2015) Direct involvement of retinoblastoma family proteins in DNA repair by non-homologous end-joining. Cell Rep 10: 2006-18

Cools T, De Veylder L (2009) DNA stress checkpoint control and plant development. Curr Opin Plant Biol 12: 23-8

Cools T, Iantcheva A, Weimer AK, Boens S, Takahashi N, Maes S, Van den Daele H, Van Isterdael G, Schnittger A, De Veylder L (2011) The Arabidopsis thaliana checkpoint kinase WEE1 protects against premature vascular differentiation during replication stress. Plant Cell 23: 1435-48

Coschi CH, Ishak CA, Gallo D, Marshall A, Talluri S, Wang J, Cecchini MJ, Martens AL, Percy V, Welch I, Boutros PC, Brown GW, Dick FA (2014) Haploinsufficiency of an RB-E2F1-Condensin II complex leads to aberrant replication and aneuploidy. Cancer Discov 4: 840-53

Cruz-Ramirez A, Diaz-Trivino S, Blilou I, Grieneisen VA, Sozzani R, Zamioudis C, Miskolczi P, Nieuwland J, Benjamins R, Dhonukshe P, Caballero-Perez J, Horvath B, Long Y, Mahonen AP, Zhang H, Xu J, Murray JA, Benfey PN, Bako L, Maree AF et al. (2012) A bistable circuit involving SCARECROW-RETINOBLASTOMA integrates cues to inform asymmetric stem cell division. Cell 150: 1002-15

Cruz-Ramirez A, Diaz-Trivino S, Wachsman G, Du Y, Arteaga-Vazquez M, Zhang H, Benjamins R, Blilou I, Neef AB, Chandler V, Scheres B (2013) A SCARECROW-RETINOBLASTOMA protein network controls protective quiescence in the Arabidopsis root stem cell organizer. PLoS Biol 11: e1001724

Culligan KM, Britt AB (2008) Both ATM and ATR promote the efficient and accurate processing of programmed meiotic double-strand breaks. Plant J 55: 629-38

Culligan KM, Robertson CE, Foreman J, Doerner P, Britt AB (2006) ATR and ATM play both distinct and additive roles in response to ionizing radiation. Plant J 48: 947-61

De Schutter K, Joubes J, Cools T, Verkest A, Corellou F, Babiychuk E, Van Der Schueren E, Beeckman T, Kushnir S, Inze D, De Veylder L (2007) Arabidopsis WEE1 kinase controls cell cycle arrest in response to activation of the DNA integrity checkpoint. Plant Cell 19: 211-25

De Veylder L, Beeckman T, Beemster GT, de Almeida Engler J, Ormenese S, Maes S, Naudts M, Van Der Schueren E, Jacqmard A, Engler G, Inze D (2002) Control of proliferation, endoreduplication and differentiation by the Arabidopsis E2Fa-DPa transcription factor. EMBO J 21: 1360-8

Dewitte W, Riou-Khamlichi C, Scofield S, Healy JM, Jacqmard A, Kilby NJ, Murray JA (2003) Altered cell cycle distribution, hyperplasia, and inhibited differentiation in Arabidopsis caused by the D-type cyclin CYCD3. Plant Cell 15: 79-92

Dewitte W, Scofield S, Alcasabas AA, Maughan SC, Menges M, Braun N, Collins C, Nieuwland J, Prinsen E, Sundaresan V, Murray JA (2007) Arabidopsis CYCD3 D-type cyclins link cell proliferation and endocycles and are rate-limiting for cytokinin responses. Proc Natl Acad Sci U S A 104: 14537-42

Dick FA, Rubin SM (2013) Molecular mechanisms underlying RB protein function. Nat Rev Mol Cell Biol 14: 297-306

Dissmeyer N, Weimer AK, Pusch S, De Schutter K, Alvim Kamei CL, Nowack MK, Novak B, Duan GL, Zhu YG, De Veylder L, Schnittger A (2009) Control of cell proliferation, organ growth, and DNA damage response operate independently of dephosphorylation of the Arabidopsis Cdk1 homolog CDKA;1. Plant Cell 21: 3641-54

Flynn RL, Zou L (2011) ATR: a master conductor of cellular responses to DNA replication stress. Trends Biochem Sci 36: 133-40

Friesner JD, Liu B, Culligan K, Britt AB (2005) Ionizing radiation-dependent gamma-H2AX focus formation requires ataxia telangiectasia mutated and ataxia telangiectasia mutated and Rad3-related. Mol Biol Cell 16: 2566-76

Fulcher N, Sablowski R (2009) Hypersensitivity to DNA damage in plant stem cell niches. Proc Natl Acad Sci U S A 106: 20984-8

Furukawa T, Curtis MJ, Tominey CM, Duong YH, Wilcox BW, Aggoune D, Hays JB, Britt AB (2010) A shared DNA-damage-response pathway for induction of stem-cell death by UVB and by gamma irradiation. DNA Repair (Amst) 9: 940-8

Gehl C, Waadt R, Kudla J, Mendel RR, Hansch R (2009) New GATEWAY vectors for high throughput analyses of protein-protein interactions by bimolecular fluorescence complementation. Mol Plant 2: 1051-8

Gutzat R, Borghi L, Gruissem W (2012) Emerging roles of RETINOBLASTOMA-RELATED proteins in evolution and plant development. Trends Plant Sci 17: 139-48

Harashima H, Dissmeyer N, Schnittger A (2013) Cell cycle control across the eukaryotic kingdom. Trends Cell Biol 23: 345-56

Harashima H, Sugimoto K (2016) Integration of developmental and environmental signals into cell proliferation and differentiation through RETINOBLASTOMA-RELATED 1. Curr Opin Plant Biol 29: 95-103

Harper JW, Elledge SJ (2007) The DNA damage response: ten years after. Mol Cell 28: 739-45

Henriques R, Magyar Z, Monardes A, Khan S, Zalejski C, Orellana J, Szabados L, de la Torre C, Koncz C, Bogre L (2010) Arabidopsis S6 kinase mutants display chromosome instability and altered RBR1-E2F pathway activity. EMBO J 29: 2979-93

Hinds PW (2014) A little pRB can lead to big problems. Cancer Discov 4: 764-5

Hoeijmakers JH (2009) DNA damage, aging, and cancer. N Engl J Med 361: 1475-85

Horvath BM, Magyar Z, Zhang Y, Hamburger AW, Bako L, Visser RG, Bachem CW, Bogre L (2006) EBP1 regulates organ size through cell growth and proliferation in plants. EMBO J 25: 4909-20

Hu Z, Cools T, De Veylder L (2015) Mechanisms Used by Plants to Cope with DNA Damage. Annu Rev Plant Biol

Ianari A, Natale T, Calo E, Ferretti E, Alesse E, Screpanti I, Haigis K, Gulino A, Lees JA (2009) Proapoptotic function of the retinoblastoma tumor suppressor protein. Cancer Cell 15: 184-94

Johnston AJ, Kirioukhova O, Barrell PJ, Rutten T, Moore JM, Baskar R, Grossniklaus U, Gruissem W (2010) Dosage-sensitive function of retinoblastoma related and convergent epigenetic control are required during the Arabidopsis life cycle. PLoS Genet 6: e1000988

Kobayashi K, Suzuki T, Iwata E, Nakamichi N, Suzuki T, Chen P, Ohtani M, Ishida T, Hosoya H, Muller S, Leviczky T, Pettko-Szandtner A, Darula Z, Iwamoto A, Nomoto M, Tada Y, Higashiyama T, Demura T, Doonan JH, Hauser MT et al. (2015) Transcriptional repression by MYB3R proteins regulates plant organ growth. EMBO J

Kuwabara A, Gruissem W (2014) Arabidopsis RETINOBLASTOMA-RELATED and Polycomb group proteins: cooperation during plant cell differentiation and development. J Exp Bot 65: 2667-76

Lang J, Smetana O, Sanchez-Calderon L, Lincker F, Genestier J, Schmit AC, Houlne G, Chaboute ME (2012) Plant gammaH2AX foci are required for proper DNA DSB repair responses and colocalize with E2F factors. New Phytol 194: 353-63

Liu L, Zhang Y, Tang S, Zhao Q, Zhang Z, Zhang H, Dong L, Guo H, Xie Q (2010) An efficient system to detect protein ubiquitination by agroinfiltration in Nicotiana benthamiana. Plant J 61: 893-903

Magyar Z, De Veylder L, Atanassova A, Bako L, Inze D, Bogre L (2005) The role of the Arabidopsis E2FB transcription factor in regulating auxin-dependent cell division. Plant Cell 17: 2527-41

Magyar Z, Horvath B, Khan S, Mohammed B, Henriques R, De Veylder L, Bako L, Scheres B, Bogre L (2012) Arabidopsis E2FA stimulates proliferation and endocycle separately through RBR-bound and RBR-free complexes. EMBO J 31: 1480-93

Nagy SK, Darula Z, Kallai BM, Bogre L, Banhegyi G, Medzihradszky KF, Horvath GV, Meszaros T (2015) Activation of AtMPK9 through autophosphorylation that makes it independent of the canonical MAPK cascades. Biochem J 467: 167-75

Naouar N, Vandepoele K, Lammens T, Casneuf T, Zeller G, van Hummelen P, Weigel D, Ratsch G, Inze D, Kuiper M, De Veylder L, Vuylsteke M (2009) Quantitative RNA expression analysis with Affymetrix Tiling 1.0R arrays identifies new E2F target genes. Plant J 57: 184-94

Narasimha AM, Kaulich M, Shapiro GS, Choi YJ, Sicinski P, Dowdy SF (2014) Cyclin D activates the Rb tumor suppressor by mono-phosphorylation. Elife 3

Nowack MK, Harashima H, Dissmeyer N, Zhao X, Bouyer D, Weimer AK, De Winter F, Yang F, Schnittger A (2012) Genetic framework of cyclin-dependent kinase function in Arabidopsis. Dev Cell 22: 1030-40

Polyn S, Willems A, De Veylder L (2015) Cell cycle entry, maintenance, and exit during plant development. Curr Opin Plant Biol 23: 1-7

Preuss SB, Britt AB (2003) A DNA-damage-induced cell cycle checkpoint in Arabidopsis. Genetics 164: 323-34

Reidt W, Wurz R, Wanieck K, Chu HH, Puchta H (2006) A homologue of the breast cancer-associated gene BARD1 is involved in DNA repair in plants. EMBO J 25: 4326-37

Ricaud L, Proux C, Renou JP, Pichon O, Fochesato S, Ortet P, Montane MH (2007) ATM-mediated transcriptional and developmental responses to gamma-rays in Arabidopsis. PLoS One 2: e430

Riou-Khamlichi C, Huntley R, Jacqmard A, Murray JA (1999) Cytokinin activation of Arabidopsis cell division through a D-type cyclin. Science 283: 1541-4

Rosen EM (2013) BRCA1 in the DNA damage response and at telomeres. Front Genet 4: 85

Sadasivam S, DeCaprio JA (2013) The DREAM complex: master coordinator of cell cycle-dependent gene expression. Nat Rev Cancer 13: 585-95

Sakamoto T, Inui YT, Uraguchi S, Yoshizumi T, Matsunaga S, Mastui M, Umeda M, Fukui K, Fujiwara T (2011) Condensin II alleviates DNA damage and is essential for tolerance of boron overload stress in Arabidopsis. Plant Cell 23: 3533-46

Schepers A, Ritzi M, Bousset K, Kremmer E, Yates JL, Harwood J, Diffley JF, Hammerschmidt W (2001) Human origin recognition complex binds to the region of the latent origin of DNA replication of Epstein-Barr virus. EMBO J 20: 4588-602

Scheres B (2007) Stem-cell niches: nursery rhymes across kingdoms. Nat Rev Mol Cell Biol 8: 345-54

Sherman MH, Bassing CH, Teitell MA (2011) Regulation of cell differentiation by the DNA damage response. Trends Cell Biol 21: 312-9

Shiloh Y (2014) ATM: expanding roles as a chief guardian of genome stability. Exp Cell Res 329: 154-61

Shiloh Y, Ziv Y (2013) The ATM protein kinase: regulating the cellular response to genotoxic stress, and more. Nat Rev Mol Cell Biol 14: 197-210

Su TT (2006) Cellular responses to DNA damage: one signal, multiple choices. Annu Rev Genet 40: 187-208

Trapp O, Seeliger K, Puchta H (2011) Homologs of breast cancer genes in plants. Front Plant Sci 2: 19

Vanstraelen M, Baloban M, Da Ines O, Cultrone A, Lammens T, Boudolf V, Brown SC, De Veylder L, Mergaert P, Kondorosi E (2009) APC/C-CCS52A complexes control meristem maintenance in the Arabidopsis root. Proc Natl Acad Sci U S A 106: 11806-11

Velez-Cruz R, Manickavinayaham S, Biswas AK, Clary RW, Premkumar T, Cole F, Johnson DG (2016) RB localizes to DNA double-strand breaks and promotes DNA end resection and homologous recombination through the recruitment of BRG1. Genes Dev 30: 2500-2512

Waterworth WM, Drury GE, Bray CM, West CE (2011) Repairing breaks in the plant genome: the importance of keeping it together. New Phytol 192: 805-22

Welch D, Hassan H, Blilou I, Immink R, Heidstra R, Scheres B (2007) Arabidopsis JACKDAW and MAGPIE zinc finger proteins delimit asymmetric cell division and stabilize tissue boundaries by restricting SHORT-ROOT action. Genes Dev 21: 2196-204

Wildwater M, Campilho A, Perez-Perez JM, Heidstra R, Blilou I, Korthout H, Chatterjee J, Mariconti L, Gruissem W, Scheres B (2005) The RETINOBLASTOMA-RELATED gene regulates stem cell maintenance in Arabidopsis roots. Cell 123: 1337-49

Xiao H, Goodrich DW (2005) The retinoblastoma tumor suppressor protein is required for efficient processing and repair of trapped topoisomerase II-DNA-cleavable complexes. Oncogene 24: 8105-13

Xiong Y, McCormack M, Li L, Hall Q, Xiang C, Sheen J (2013) Glucose-TOR signalling reprograms the transcriptome and activates meristems. Nature 496: 181-6

Yi D, Alvim Kamei CL, Cools T, Vanderauwera S, Takahashi N, Okushima Y, Eekhout T, Yoshiyama KO, Larkin J, Van den Daele H, Conklin P, Britt A, Umeda M, De Veylder L (2014) The Arabidopsis SIAMESE-RELATED Cyclin-Dependent Kinase Inhibitors SMR5 and SMR7 Regulate the DNA Damage Checkpoint in Response to Reactive Oxygen Species. Plant Cell 26: 296-309

Yoshiyama K, Conklin PA, Huefner ND, Britt AB (2009) Suppressor of gamma response 1 (SOG1) encodes a putative transcription factor governing multiple responses to DNA damage. Proc Natl Acad Sci U S A 106: 12843-8

Yoshiyama KO, Kobayashi J, Ogita N, Ueda M, Kimura S, Maki H, Umeda M (2013a) ATM-mediated phosphorylation of SOG1 is essential for the DNA damage response in Arabidopsis. EMBO Rep 14: 817-22

Yoshiyama KO, Sakaguchi K, Kimura S (2013b) DNA damage response in plants: conserved and variable response compared to animals. Biology (Basel) 2: 1338-56

Zalmas LP, Coutts AS, Helleday T, La Thangue NB (2013) E2F-7 couples DNA damage-dependent transcription with the DNA repair process. Cell Cycle 12: 3037-51

Zebell SG, Dong X (2015) Cell-Cycle Regulators and Cell Death in Immunity. Cell Host Microbe 18: 402-7

FIGURE LEGENDS

Fig 1. Silencing of RBR and *CYCD3.1* overexpression both promote S-phase entry but affect cell death response and DNA damage accumulation differently.

(A) Representative confocal laser scanning microscopy (CM) images of whole mount EdU labelled roots from 6 days-old (das) seedlings of Col-0, *amiRBR* and Col-0*(CYCD3.1OE*) lines with EdU (green) and DAPI (DNA, blue) staining. In the *amiRBR* and Col-0*(CYCD3.1OE)* lines, the region of extra columella stem cell layers is labelled with a green bar in merged images. White vertical bar shows the region of cells where EdU counting was carried out.

(**B**) CM images of propidium-iodide (PI) stained root-tips from 12 das seedling; genotypes indicated as in (**A)**. In (**A, B**) images were taken in single median section, scale bar: 50μM, arrow: QC position in each image.

(**C**) Number of EdU labelled cells as shown in (**A**) were counted in the of epidermis, cortex and endodermis cell layers on both sides of the root. In each case, 10 roots (6 das) were quantified.

(**D**) Cell death response in 6 and 12 das seedlings, total number of dead columella stem cells (CSC) and lateral root cap initials (LRC) and their descendants were counted in median sections as shown in (**B**), n>2, N>15. Note, that in Col-0*(CYCD3.1OE)* only 1-2 dead cells were detected in the analysed population. Quantification of the dead cell area in *amiRBR* is shown in Fig 2C.

(**E**) Frequency of γH2AX labelled nuclei per total number of DAPI positive nuclei (%) n=2, N>6 root of 6das seedlings, analysed nuclei>1000.

(**F**) Representative CM images (single section) of γH2AX immune-labelled cells of root-tips from Col-0, *amiRBR* and Col-0*(CYCD3.1OE*). DAPI (blue), scale bar: 5μM.

Data information**: (C-E**) values represent means with standard deviation (s.d.). *a*: indicates significant difference around 1% confidence using Student's *t*-test (here and following Figs) comparing *amiRBR* and Col-0*(CYCD3.1OE)* to Col-0. In (**D**) *b*: 99% significance ($p<0.01$) between time points and in **(E**) *ab*: 99% significance ($p<0.01$) to Col-0 and *amiRBR*. (n=biological repeat, N=sample per biological repeat, here and following Figs).

Fig 2. Genotoxic stress upon RBR silencing leads to hypersensitive DNA damage response.

(**A**) Representative (CM) images of Col-0, *rRBr* and *amiRBR* root-tips of 6/7 days old seedlings after 16 h mitomycin (+MMC) and 20 h zeocin treatment compared to non-treated samples (Control).

(**B and C**) Cell death was quantified (**B**) by the number of the dead columella and lateral root cap stem cells (CSC, LRC) and their daughter cells, and (**C**) by measuring the area of dead vasculature above the QC in the presence of MMC for 16 h and zeocin for 20 h.

(D) Representative (CM) images of Col-0 and *amiRBR* root-tips of 6/7 days old seedlings after 16 h hydroxyurea (HU) treatment compared to non-treated samples (Control shown in **A**).

(E) Representative (CM) images of nuclei (single section) of Col-0 and *amiRBR* 6 das root-tips after 16 h of MMC treatment immune-labelled for γH2AX (green). DAPI (blue), scale bar: 5 μm.

(F) Frequency (%) of γH2AX foci harbouring nuclei compared to total nuclei in 6das Col-0 and *amiRBR* root-tip after 16 h MMC treatment compared to non-treated samples.

Data information: In (**A** and **D**) Arrow indicates position of QC, scale bar: 50mM. In (**B, C** and **F**) values represent mean with standard error, data are combined from n=3 biological repeats, N>15 roots for (**B and C**) and N>5 in (**F**) of *amiRBR* and Col0, total nuclei>1000. *a*: indicates significant difference within the 5% to 1%, statistical confidence interval using Student's *t*-test between *amiRBR* and *rRBr* vs Col-0, and *b*: between treated vs non-treated samples.

Fig 3. RBR and E2FA nuclear focus formation depends on ATM/ATR kinases and coincide with γH2AX positive sites upon MMC and zeocin treatments

(A) Representative CM images (single section) of nuclei with RBR foci at the γH2AX positive sites in Col-0 upon 16 h of MMC and 3 h zeocin treatment (white arrowheads); diffuse nuclear RBR signal is shown in the untreated control (RBR: green, γH2AX: red, DAPI:blue).

(**B**) Partial co-localisation of RBR and γH2AX foci shown on Imaris section of the nucleus (RBR: green, γH2AX: red).

(**C**) Representative CM images (single section) of nuclei showing accumulation of RBR (red) and E2FA-GFP (green) in the same nuclear foci (white arrowheads) after 16 h MMC and 3 h zeocin treatment (RBR: red, E2FA-GFP: green, DAPI: blue). RBR and E2FA-GFP focus formation was not detected in untreated cells (Control) or upon inhibition of ATM and ATR kinases (IATM+IATR+MMC). The activity of IATM and IATR inhibitors was followed on cell death response

(D) Imaris section of a nucleus showing co-localisation of RBR (red) and E2FA-GFP (green) in foci (DAPI: blue). In (**B and D**), main panel (z) shows a single z–stack of the nucleus, right panel (y-z) shows cross-section by y plane perpendicular to z plane in the main panel, lower panel (x-z) illustrates cross-section by x plane perpendicular to z plane in the main panel. Scale bar: 1 μm; scale bar of magnified insets: 0,5 μm.

(**E**) The range of Pearson Correlation Coefficients (PCCs) of RBR/E2FA and RBR/γH2AX positive foci formed after 16 h MMC. PCCs are visualized in quartiles of ranked data (n = 30). While RBR/E2FA co-localised in foci with high mean value of PCCs = 0.82, the RBR/γH2AX in foci showed PCCs ranging from 0.1 (side by side co-localisation) to 0.75 (partial co-localisation).

(F) The effect of IATM and IATR inhibitors on cell death response upon 16 h MMC treatment in Col-0 was quantified by the number of columella stem cells (CSC) and lateral cap stem cells (LRC) and their descendants. Values represent mean with standard deviation, n=2 biological repeats, N>15 roots for each, *a*: indicates significant difference within the 5% to 1%, statistical confidence interval using Student's *t*-test comparing samples treated with inhibitors (single or combined) and MMC to MMC only.

(**G**) Representative CM image (single section) of a nucleus shows localisation of RBR and E2FA to a γH2AX positive site after 16 h MMC treatment (white arrowheads, RBR: violet, γH2AX: red, E2FA-GFP: green, DAPI; blue).

Data information: In the intensity profiles (**A, C** and **G)**, the x axis shows length in μm measured from 1 and y axis illustrates relative intensity. Scale bar: 2 μm.

Fig 4. AtBRCA1 and RBR are recruited to γH2AX foci and partially co-localise upon genotoxic stress, and locate to foci independent of each other.

(**A**) Representative CM images of PI-stained root-tips of Col-0, *Atbrca1*-1 (0, 16 h) and *Atbrca1-1*(*AtBRCA1*$_{pro}$*:AtBRCA1*$_{gen}$*:GFP*) seedlings after 0, 4 and 16 h MMC treatment. Arrow indicates position of QC, scale bar: 50 μm. Inset in the last image illustrates an enlarged nucleus with pronounced speckles.

(**B**) CM images of PI-stained root-tips of *rRBr;*(AtBRCA1:GFP) showing AtBRCA-GFP accumulation into foci in QC and the stem cell niche labelled with green arrowheads. Top and bottom images represent different root-tips. Scale bar: 50 μm.

(C) Representative CM images of nuclei (single section) with triple immune-labelling for RBR (violet), γH2AX (red) and AtBRCA1 (green) and stained for DAPI (blue) showing co-localisation of AtBRCA1-GFP with γH2AX (arrowheads), RBR with γH2AX (arrowheads) and RBR, γH2AX and BRCA-GFP (arrowheads) after 16 h MMC treatment. In the presence of ATM and ATR inhibitors (IATM+IATR+MMC) the γH2AX and AtBRCA1-GFP nuclear signals and RBR foci formation were abolished. See also Table 1 for statistics.

(D) Representative CM image (single section) of RBR foci localized with γH2AX positive sites (arrowheads) in nucleus of *Atbrca1-1* root meristematic cells after 16 h of MMC treatment. (RBR: green, γH2AX: red, DAPI: blue).

In (**C and D**), intensity profiles: x axis shows length in μm measured from 1; y axis shows relative intensity. Scale bar 2 μm. N>3, n=3.

Fig 5. RBR and AtBRCA1 proteins can physically interact.

(A) Co-immuno precipitation of RBR with AtBRCA1 and E2FA proteins; Control:streptavidin beads, RBR: streptavidin beads bound with RBR-biotin, AB-GST: GST (anti-glutathione-S-transferase) antibody, E A-POD: ExtrAvidin-POD (peroxidase-conjugated streptavidin) labelling RBR-biotin containing complexes. GST-BRCA1: GST-labelled AtBRCA1 and GST-E2FA: GST-labelled E2FA proteins, in the input of the wheat-germ extract.

(B) BiFC assay in planta reveals physical interaction between AtBRCA1 and RBR (BRCA1-N/RBR-C). The RBR-N/SCR-C pair was used as a positive -, and BRCA1-N/SCR-C pair as a negative control. Young, growing tobacco leaves were infiltrated and analysed 36-48 h after infiltration. Scale bar: 50 μm, SCR: SCARECROW transcription factor.

Fig 6. RBR and AtBRCA1 may act in a common process during DDR.

(**A**) Representative (CM) images of nuclei (single section) of *amiRBR*, *Atbrca1-1*, and *amiRBR;Atbrca1-1* 6das root tips immuno-labelled for γH2AX (green), DAPI (blue), Scale bar: 5 μm.

(B) Frequency (%) of γH2AX labelled nuclei to total DAPI stained nuclei in Col-0, *amiRBR*, *Atbrca1-1, amiRBR;Atbrca1-1* grown in normal conditions. Graphs represent means with s.d., n=3, and total nuclei>1000. *a*: indicates significant difference within the 1%, statistical confidence interval using Student's *t*-test between *amiRBR, Atbrca1-1, amiRBR;Atbrca1-1* vs Col-0.

(**C**) CM images of PI-stained root-tips from *amiRBR*, *amiRBR;brca1-1* and *amiRBR;brca1-3* of 12 das seedlings. Scale bar: 20 μm, arrow: QC position in each image.

(**D**) Cell death response of *amiRBR*, *amiRBR;brca1-1*, *amiRBR;brca1-3* seedlings at 4, 6, and 12 das. Values represent means with s.d., N>15 for each mutant and Col-0, (n=3-4) *a*: p<0.01 between the given genotype and *Atbrca1-1*, which did not develop cell death at any time point. *b*:p<0.01 comparison between cross and *amiRBR*. In (**D**) the total number of dead columella stem and daughter cells (CSC), lateral root cap initials and their descendants (LRC) counted in median sections as shown in (**C**).

Fig 7. Genes regulated by RBR are annotated to nucleosome assembly, replication and DDR; RBR protein is enriched on the AtBRCA1 promoter

(**A**) The pie chart represents the major processes regulated by RBR.

(**B-C**) show the validation of transcriptome analysis for a selected set up- and downregulated genes upon RBR silencing, respectively, using qRT-PCR on dissected root-tips of 4 days-old *rRBr* and Col-0 seedlings.

(D) illustrates that genes showing differential expression upon local RBR silencing also are de-repressed in the constitutively silenced *amiRBR* line. Graph represent qRT-PCR on 4 days-old seedling material.

(E) Schematic representation of the *AtBRCA1* promoter; black lines with numbers indicate the position and length of the amplified regions by qPCR analysis, the position of the start codon (ATG), the stop codon of the upstream neighbouring transcript and the position of putative E2F elements (red arrow-heads) on the + and - strand, at position 234- and -151, respectively are indicated. Position of amplified regions: 1:-383 to -248; 2:-238 to -78; and 3: +313 to +455; positions are numbered from ATG (+1).

(**F**) Chromatin-Immuno Precipitation (ChIP) using RBR antibody; the graph shows fold enrichment calculated as a ratio of chromatin bound to the numbered section of the promoter with or without antibody. Values represent mean of three biological replicates with standard error, *a*:p<0,01 compared to the negative control and *b*:p<0,01, compared to the positive control. PCNA1 promoter was used. as a positive- and IR (an intergenic region between At3g03360-70) as a negative control. the enrichment on IR was arbitrarily set to 1. Numbers 1,2,3 on x axis refer to the regions labelled in (**E**).

Data information: In (**B-D)** Values represent mean of fold change normalised to values of the relevant genes from Col-0, error bar: +/- s.d., n=2, N>100. All of the values were in the 1%, statistical confidence interval using Student's *t*-test. Abbreviations of genes in Appendix Supplementary Information, TableS1 and primers used in this study TableS3.

(**F**) ChIP using GFP antibody to chromatin isolated from Col-0(AtE2FA-GFP) seedlings, graph shows fold enrichment on the AtBRCA1 promoter region 2 without and upon genotoxic treatment (MMC 16 h). Graph shows a representative experiment. *a*: p<0.01 without MMC, *b*:p<0.01 in MMC compared to the non-treated and IR control. In (**E**) and (**F**) the enrichment on IR was arbitrarily set to 1.

Fig 8. Spontaneous cell death upon RBR silencing is suppressed by E2FA and DNA damage response upon genotoxic stress is dependent on E2FA.

(**A**) Relative transcript level of *AtBRCA1* in *amiRBR*, *e2fa-1*, *e2fa-2*, their double mutants and *e2fb-1*, *e2fb -2* compared to Col-0, where the level of expression was set arbitrarily to 1.

(**B**) Relative transcript level of *AtBRCA1* in Col-0, *e2fa-1*, *e2fb-1* and *e2fb -2* without and upon 16h MMC treatment. All the values are compared to the expression level measured in non-induced Col-0 which was set to 1.

In (**A** and **B**) values represent mean +/-s.d., n>2, N>100 in each experiment. *a*:p<0.05 significance using Student *t*-test, comparing single mutant to Col-0 and in (**B**) *b*:p<0.05, comparing values upon MMC treatment.

(**C**) ChIP using GFP antibody to chromatin isolated from Col-0(AtE2FA-GFP) seedlings, graph shows fold enrichment on the *AtBRCA1* promoter region 2 without and upon genotoxic treatment (MMC, 16 h). Graph illustrates a representative experiment. *a*: p<0.01 without MMC, *b*:p<0.01 in MMC compared to the non-treated and IR control. The enrichment on IR was arbitrarily set to 1.

(**D**) Quantitative analysis of cell death response in Col-0, *e2fa-1*, *e2fa-2*, *amiRBR, amiRBR;e2fa-1* and *amiRBR;e2fa-2* mutants at 6 and 12 das. Values represent mean +/- s.d., at least two biological replicates testing more than 20 seedlings for each mutant. Note, the absence and insignificant number of spontaneous cell death in the distal stem cell niche in Col-0 and *e2fa* mutants, respectively, at these time points. *a*:p<0.05 significance comparing single mutant to Col-0 and *b*:p<0.05 comparing double mutants to *amiRBR*. (CSC: columella stem cells, LRC; lateral root cap initials and their descendents).

(**F**) CM images of PI-stained root-tips in non-treated *e2fa-1* mutant, and MMC treated Col-0 and *e2fa-1* (6das). Images were taken in median section, scale bar: 50 μM, arrow: QC position in each image.

Fig 9. DNA damage response upon RBR silencing is independent of SOG1.

(A) CM images of PI-stained root-tips (12 das seedlings) from the genotypes indicated.

(**B**) Cell death response from 6 and 12 das seedlings, total number of dead columella stem cells (CSC), lateral root cap initials (LRC) and their descendants were counted as shown in **(A**). Note, that neither Col-0 at 6 das and nor *sog1-1* at 6 and 12 das showed cell death. *a*:p<0.05 at 6das, *b*:p<0.05 at 12 das mutant vs Col-0. Value represents mean +/-s.d., n>3, N>15 for each mutant and Col-0. Explanation to the symbols in graph also holds for **C** and **D**.

(**C**) Relative expression level of DDR genes in *sog1-1*, *amiRBR* and *amiRBR,sog1-1* lines (6 das) compared to Col-0 (6 das), where the level of expression for each gene was set arbitrarily to 1. *a*:p<0.05, mutants compared to Col-0

(**D**) Transcriptional induction of the indicated genes is depicted as fold change comparing MMC (16hrs) to non-treated samples of Col-0, *sog1-1*, *amiRBR* and *amiRBR,sog1-1*. *a*: p<0.05 *amiRBR* vs Col-0 and *b*:p<0.05 *amiRBR,sog1-1* to *sog1-1*.

Data Information: In (**C**) and (**D**) 6 das seedlings were analysed, data represent means with +/-s.d.; Significance was determined by Student *t*-test, at least three biological replicates, in each case around 100 seedlings for each mutants. For *amiRBR,sog1-1* the mean was calculated from the analysis of 6 independent transformants (T2 generation).

Expanded View

Fig EV1. Both, local silencing of RBR and overexpression of E2FA-DPA and E2FB-DPA results in extra S-phase entry but only RBR silencing triggers cell death response.

(**A**) Differential interference contrast (DIC) microscopy images using Lugol staining to detect differentiated columella cells. Note, the increased number of layer columella cell layers upon local reduction of RBR. Black arrow indicates the position of the dissection used to collect material for micro-array analysis.

(**B**) Confocal microscopy images (CM) of root-tips after EdU staining (green, 2 h) at 4 das counterstained with DAPI (blue) and at 6 and 10 das using bright field.

(**C**) CM images of PI stained root samples from *rRBr* seedlings showing accumulation of cell death in time.

(**D**) Representative CM images of whole mount EdU labelled (green) root-tips of 6 das Col-0, Col-0*(E2FA/DPAOE)* and Col-0*(E2FB/DPAOE)* seedlings, DNA was stained by DAPI.

(**E**) Representative PI- stained CM images of 12 das root-tips from the genotypes indicated. Note, that no cell death response was detected at any time point analysed.

In (**A and E**) images were taken in median section, scalebar: 50μM, genotype as indicated in the images, white arrow: QC position in each image.

Fig EV2. RBR nuclear foci can localize with condensed heterochromatin and CenH3.

(A) Representative CM images of nuclei (single section) of Col-0 6 das root-tips after 16 h of MMC treatment immuno-labelled for RBR (green), γH2AX (red), DAPI (blue). RBR

foci localized at γH2AX positive sites and with DNA heterochromatin spots labelled by arrowheads, while RBR foci localised independently of condensed chromatin are marked by arrows.

(B) Representative CM image of nucleus (single section) showing localization of RBR foci to CenH3 labelled region (arrowheads) in 6 das Col-0 root tips after 16 h of MMC treatment. (RBR: green, CenH3: red, DAPI: blue).

In (**A and B**), intensity profiles: x axis shows length in μm measured from 1; y axis shows relative intensity. Scale bar 2 μm. N>3, n=3.

Fig EV3. The *Atbrca1-3* mutant, similarly to *Atbrca1-1*, also shows hypersensitivity upon genotoxic stress.

(A) Position of the T-DNA insertion in *Atbrca1-1* (Reidt et. al., 2006) and *Atbrca1-3* mutans. Given sequence indicates the insertion in *Atbrca1-3,* difference in letter type shows the exon-intron border. Arrows depict position of forward (qF) and reverse (qR) primers used for qRT-PCR reactions.

(B) Expression level of the *AtBRCA1* transcript in Col-0, *Atbrca1-1* and *Atbrca1-3* alleles compared to the *AtACTIN2* transcript level in Col-0 in normal growth conditions. To control the inducibility of the transgenes, the alleles and Col-0 were treated with MMC (+) and compared to non-treated seedlings (-). As the graph shows genotoxic stress influenced the *AtBRCA1* transcript level only in the control, but not in the alleles. However, neither of the *Atbrca1* alleles are null alleles.

(**C**) CM images of PI stained root-tips of Col-0, *Atbrca1-1* and *Atbrca1-3* 6 das seedlings grown without (-MMC) and treated with MMC (+MMC) for 16 h. Scale bar: 20μm, arrow: QC position in each image.

(D and E) Functional analysis of the (*AtBRCA1*$_{pro}$*:AtBRCA1*$_{gen}$*:GFP*) construct following cell death response in the introgressed line, *Atbrca1-1*(pgBRCA:GFP) compared to Col-0, *Atbrca1-1* and *Atbrca1-3***. (D)** Cell death response was quantified in the distal stem cell region after 16 h MMC treatment. Dead columella stem and daughter cells (CSC) and lateral root initials and their descendants (LRC) were counted in median section as shown in (**C**).

(**E**) Ratio of Pi-stained area in the proximal meristem comparing mutants and the complementing line to Col-0. Pi-stained area was measured in each experiment from N>15 mutants and Col-0, then means and ratio was calculated. Finally, the mean of the different experiments/ratios (n=3-4) was calculated and depicted.

Data Information: In (**D** and **E**) values represent means with standard deviation. *a*: indicates significant difference around 1% confidence using Student's *t*-test comparing

Atbrca1-1 and *Atbrca1-3* to Col-0, and *b*: 99% significance between *Atbrca1-1*(AtBRCA1:GFP) and *Atbrca1-1,*

Fig EV4. Lack of AtBRCA1 in conjunction with *RBR* silencing results in partially penetrant developmental arrest and suppress cell death response, but does not influence extra stem cell division and S-phase entry induced by *RBR* silencing in surviving individuals.

(**A**) Segregation (47 severe/49 survival) and growth habit of *amiRBR;Atbrca1-1* homozygous seedlings (F3).

(**B**) Developmental defects in germinating seedlings, arrowheads point to missing primary leaves.

(**C**) Relative transcript level of *AtBRCA1* in *amiRBR*, *Atbrca1-1* and *amiRBR;brca1-1* compared to Col-0, where the level of expression was set arbitrarily to 1 in non-treated samples. Upon MMC treatment the graph shows the ratio of expression between treated to non-treated samples. Values represent mean +/-s.d., n>2, N>100. *a*:p<0.05.

(**D**) Frequency (%) of EdU labelled nuclei (10min pulse) compared to total DAPI stained nuclei, *a*: p<0,001, all compared to Col-0, n>2, N>10, Error bars: +/- s.d.

(E) WOX5*pro*-WOX5*gen*-3xGFP expression in the mutant lines showing QC division in the *amiRBR;brca1-1* compared to Col-0 and *Atbrca1-1*.

(**F**) Confocal images of *amiRBR* and *amiRBR;brca1-1 r*oot-tips of 12 das seedlings showing collumella and stem cell layers (white dots), arrow: QC position. Inset is showing the incorporation and presence of the *amiRBR* construct. Scale bar: 20μM.

(G) Quantification of the number of columella and stem cell layers of 4, 6 and 12 days-old roots from *amiRBR*, *amiRBR;brca1-1* and Col-0. Values represent means +/-: s.d, N>15 for each mutant and Col-0, (n=3-4) *a*: p<0.01 between the given genotype and Col-0 at a given time point.

Fig EV5. Both transcription of *AtBRCA1* and *SMR4* upon RBR silencing and cell death response upon genotoxic stress are dependent of E2FA.

(A) Position of different T-DNA insertions in AtE2FA, colours represent different domains: dark blue: N-terminal, light blue: DNA binding domain, red: dimerisation domain, purple: marked box, lilac: transactivation domain and yellow: RBR binding domain, drawing based on Magyar et.al., (2012).

(**B**) Relative transcript level of RBR in *amiRBR* and double mutants

(**C**) Cell death response in MMC treated, 6 das seedlings of different *e2fa* alleles; total number of dead columella stem cells (CSC), lateral root cap initials (LRC) and their descendants were counted.

(**D**) Quantification of cell death by measuring the area of dead vasculature (uM^2) in the presence of MMC for 16 h. No cell death response was observed in non-treated samples.

In (**C** and **D**) bars represent mean +/-s.d., n>2, N>10. *a*:p<0.05 significance between different *e2fa mutants* vs Col-0.

(**E**) Relative transcript level of *SMR4*, *SMR5, RAD51* and *PARP2* in *amiRBR, e2fa-1, e2fa-2* and double mutants compared to Col-0, where the level of expression was set arbitrarily to 1. *a*:p<0.05 significance between mutant vs Col-0, values represent mean of relative expression, +/-s.d., n>2, N>100.

Fig EV6. Hypersensitive cell death response after genotoxic stress only partially depends on SOG1 in upon RBR silencing.

(A) CM images of PI-stained root-tips from *sog1-1*, *amiRBR* and *amiRBR,sog1-1* lines compared to Col-0 as indicated above the columns. Images were taken in median section of 6 das seedlings treated with and without MMC (10µg/ml).

(B) Representative images of 9 das seedlings showing cell death response after hydroxyurea (+HU, 1mM) or zeocin (+zeo, 20µg/ml) treatment.

In (**A** and **B**) scale bar: 50µM, arrow: QC position in each image.

(**C**) Relative *RBR* transcript level in *amiRBR* and *amiRBR,sog1-1* lines, taking mean of several independent lines. *a*:p<0.05 significance genotypes vs Col-0,

(**D)** Cell death response upon MMC treatment in *sog1-1*, *amiRBR* and *amiRBR,sog1-1* lines compared to Col-0. The total number of dead columella stem and daughter cells (CSC), lateral root cap initials (LRC) and their descendants were counted in median section as shown in (**A**). *a*:p<0.05 significance genotypes vs Col-0, *b*: p<0.05 comparison of samples treated to non-treated counterparts, *c*:p<0.05 significance between *amiRBR* vs. *amiRBR,sog1-1*. Note, that Col-0 at 6 das and *sog1-1* at 6 and 12 das developed no dead cells. Value represents mean +/-s.d., n=3, N>15 for each mutant and Col-0.

(**B**) No spontaneous cell death response was detected after 24h β-estradiol induction, arrow indicates QC position.

Table 1

Number and ratio of nuclei showing co-localisation of γH2AX, RBR and/or AtBRCA1

	Number of nuclei					Ratio	
	Root1	Root2	Root3	Mean	StDv	Mean (%)	StDv
γH2AX (total)	156	144	152	151	6.1	100%	
γH2AX+ RBR	37	56	45	46	9.5	27%	3%
γH2AX+AtBRCA1	32	42	38	37	5.0	25%	4%
γH2AX+AtBRCA1+RBR	12	14	15	14	1.5	9%	1%

Figure 1

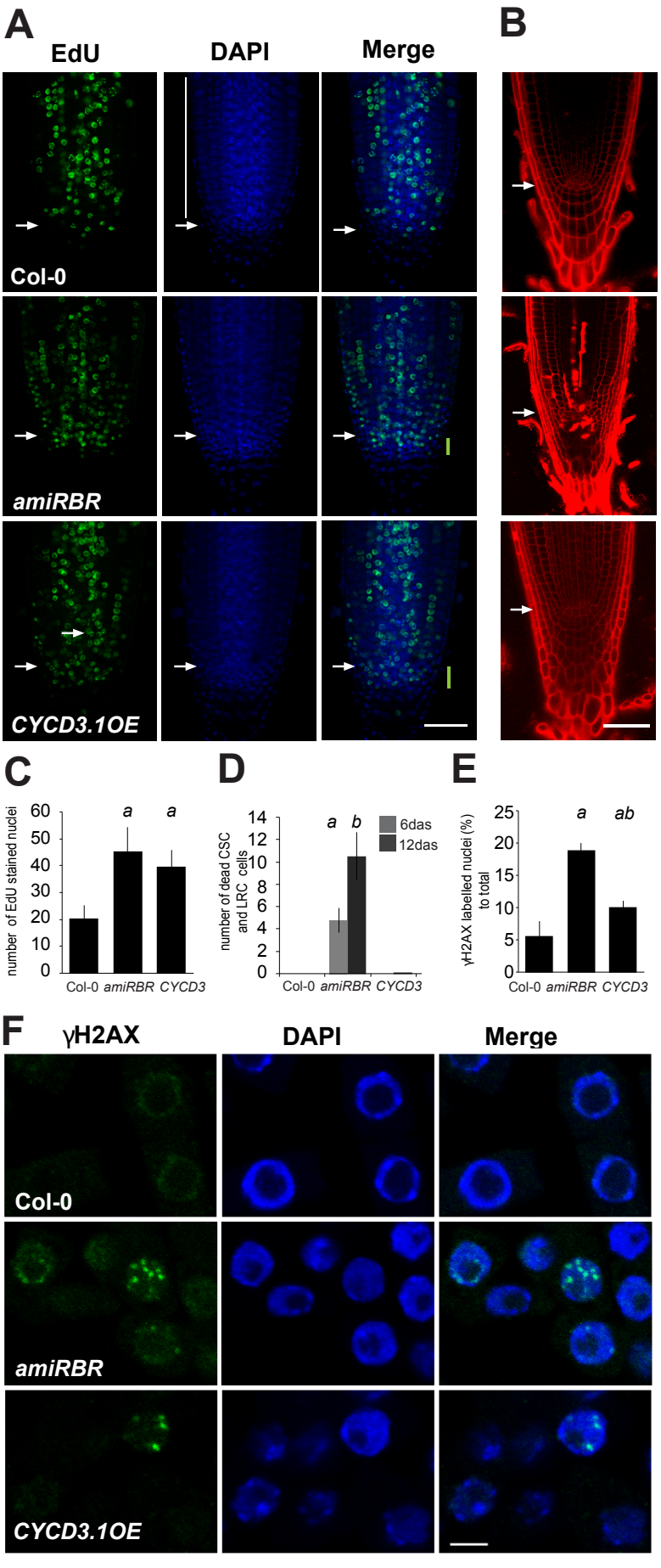
A
EdU
DAPI
Merge
B
Col-0
amiRBR
CYCD3.1OE
C
number of EdU stained nuclei
60
50
40
30
20
10
0
a
a
Col-0
amiRBR
CYCD3
D
number of dead CSC and LRC cells
14
12
10
8
6
4
2
0
a
b
6das
12das
Col-0
amiRBR
CYCD3
E
γH2AX labelled nuclei (%) to total
25
20
15
10
5
0
a
ab
Col-0
amiRBR
CYCD3
F
γH2AX
DAPI
Merge
Col-0
amiRBR
CYCD3.1OE

Figure 2

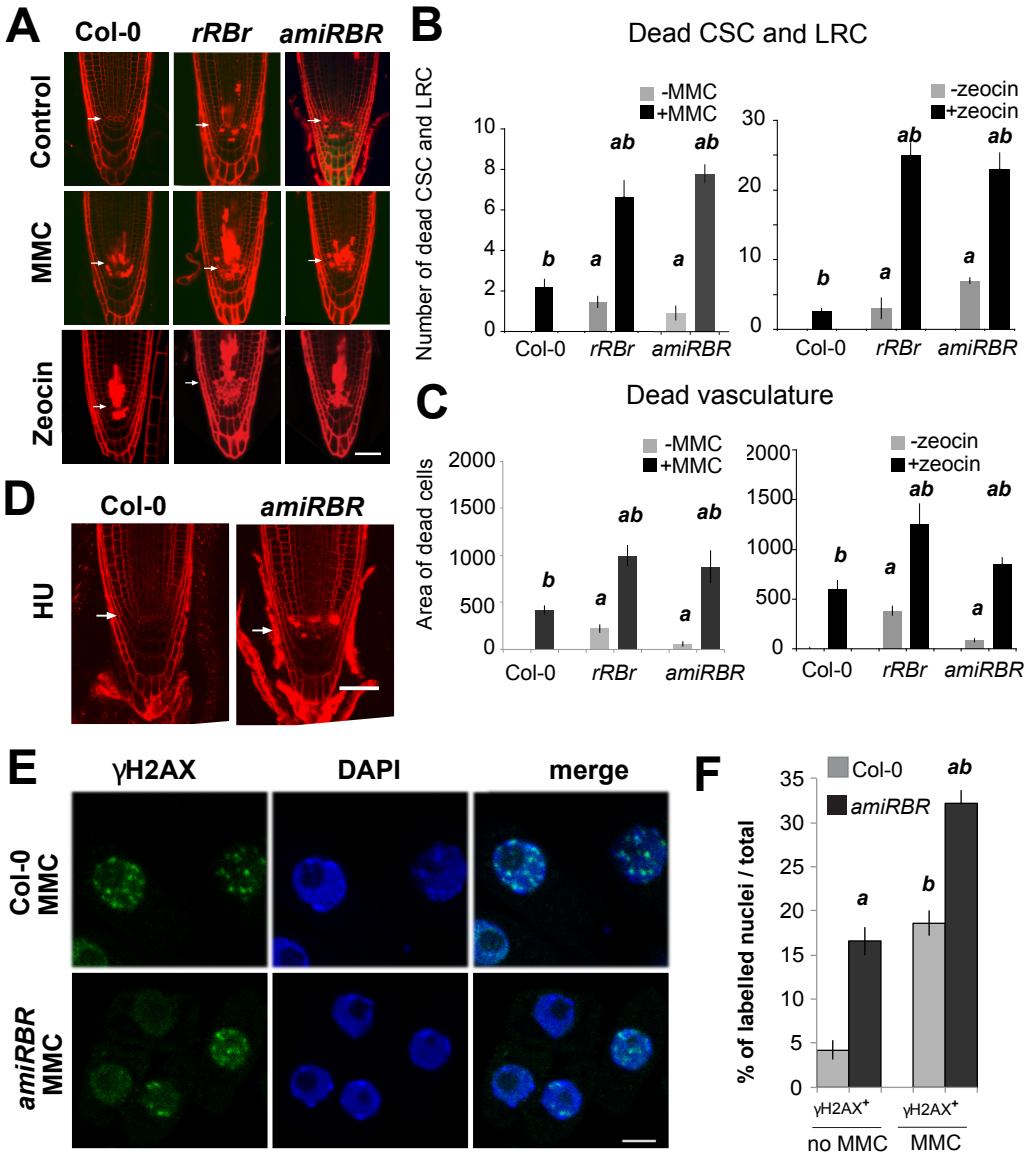
A
Col-0
rRBr
amiRBR
Control
MMC
Zeocin
B
Dead CSC and LRC
Number of dead CSC and LRC
-MMC
+MMC
-zeocin
+zeocin
Col-0
rRBr
amiRBR
C
Dead vasculature
Area of dead cells
D
Col-0
amiRBR
HU
E
γH2AX
DAPI
merge
Col-0 MMC
amiRBR MMC
F
Col-0
amiRBR
% of labelled nuclei / total
γH2AX+
no MMC
MMC

Figure 3

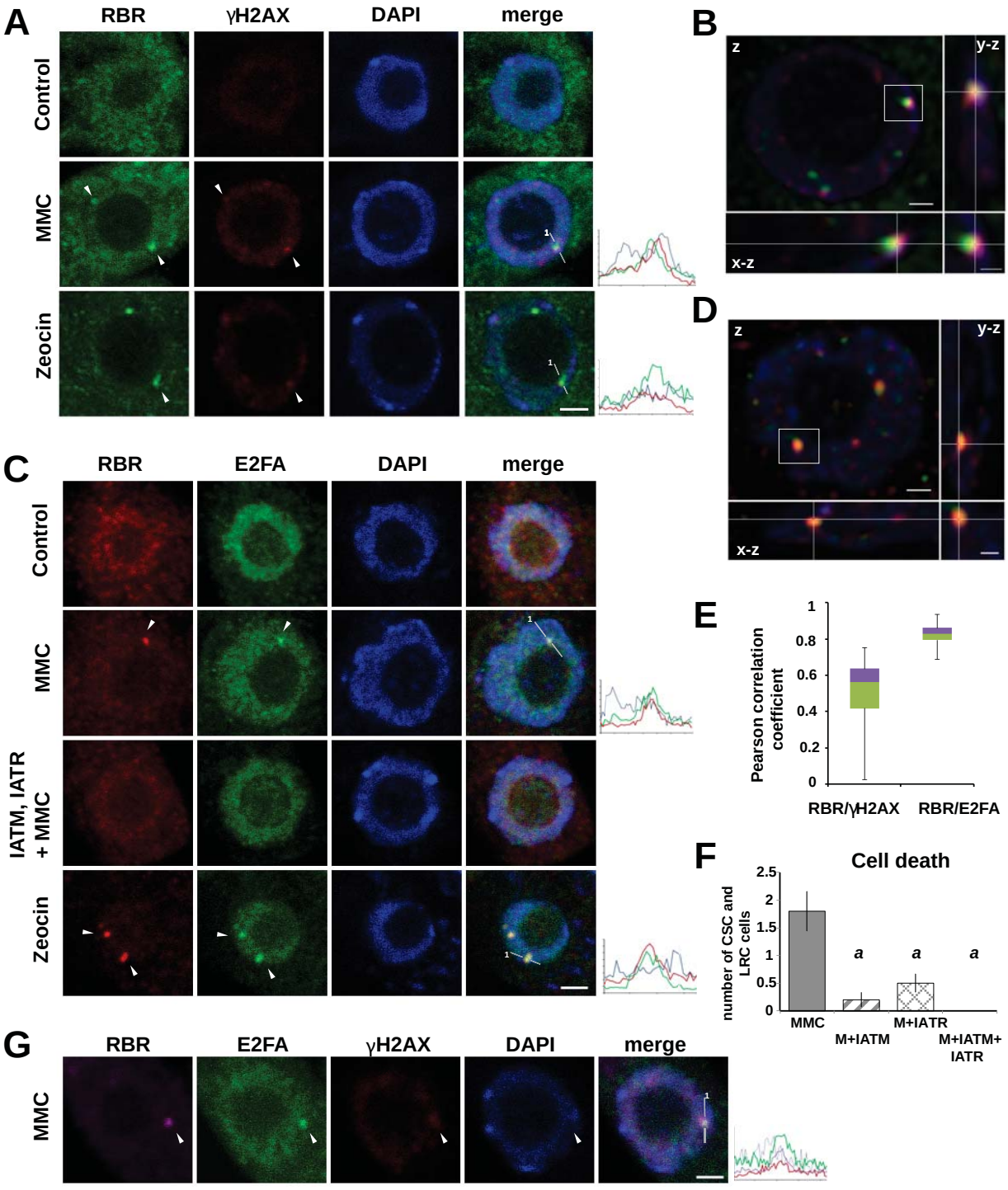
A
RBR
γH2AX
DAPI
merge
Control
MMC
Zeocin
B
z
y-z
x-z
D
z
y-z
x-z
C
RBR
E2FA
DAPI
merge
Control
MMC
IATM, IATR + MMC
Zeocin
E
Pearson correlation coefficient
1
0.8
0.6
0.4
0.2
0
RBR/γH2AX
RBR/E2FA
F
Cell death
number of CSC and LRC cells
2.5
2
1.5
1
0.5
0
a
a
a
MMC
M+IATM
M+IATR
M+IATM+ IATR
G
RBR
E2FA
γH2AX
DAPI
merge
MMC

Figure 4

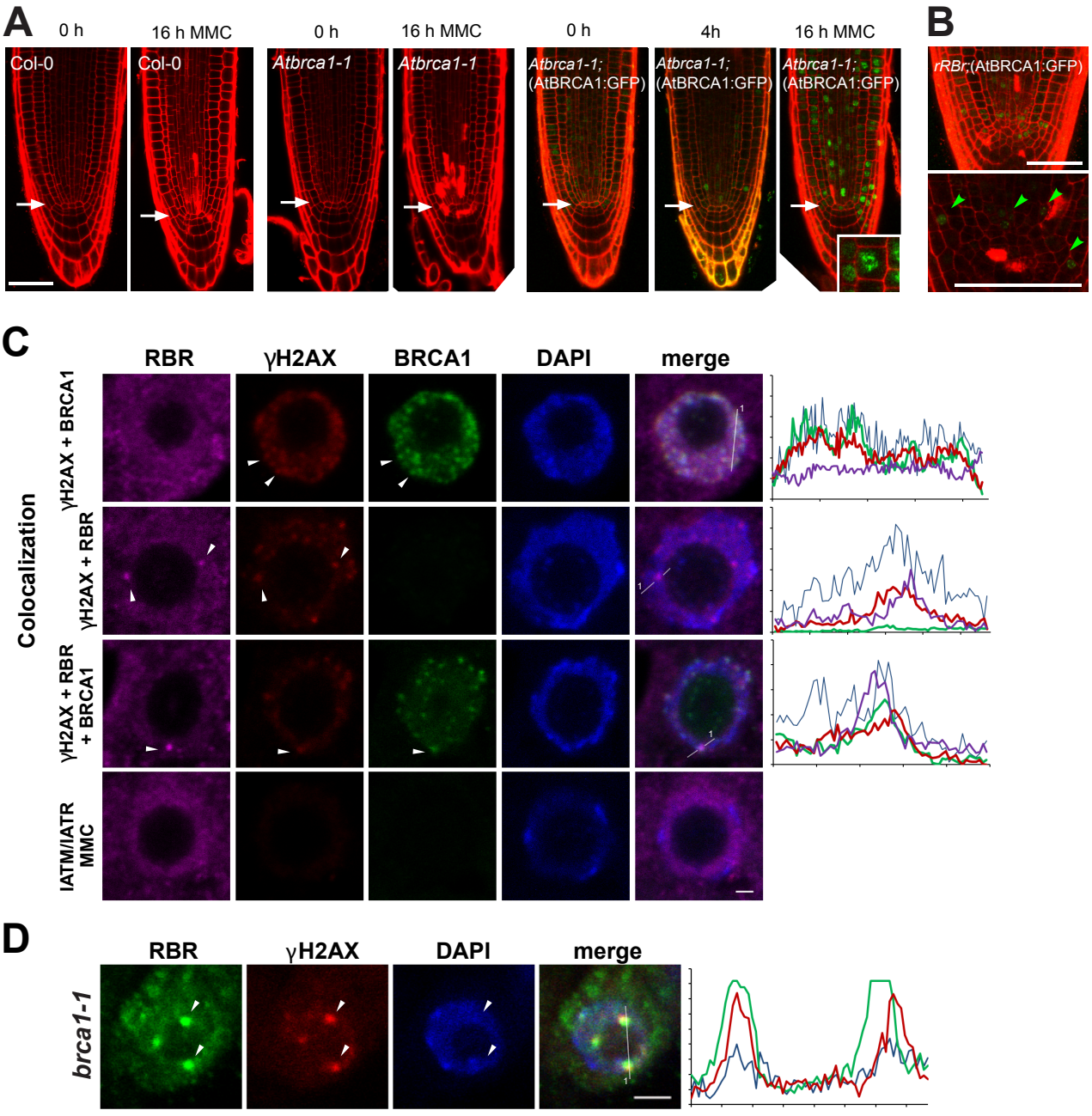
A
0 h
16 h MMC
0 h
16 h MMC
0 h
4h
16 h MMC
Col-0
Col-0
Atbrca1-1
Atbrca1-1
Atbrca1-1; (AtBRCA1:GFP)
Atbrca1-1; (AtBRCA1:GFP)
Atbrca1-1; (AtBRCA1:GFP)
B
rRBr;(AtBRCA1:GFP)
C
RBR
γH2AX
BRCA1
DAPI
merge
Colocalization
γH2AX + BRCA1
γH2AX + RBR
γH2AX + RBR + BRCA1
IATM/IATR MMC
D
RBR
γH2AX
DAPI
merge
brca1-1

Figure 5

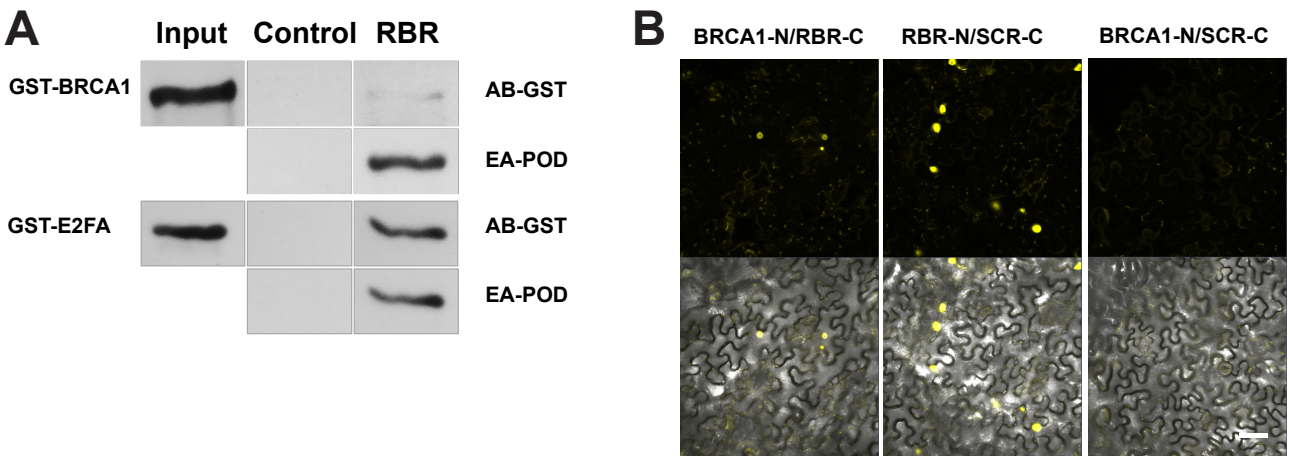
A
Input
Control
RBR
GST-BRCA1
AB-GST
EA-POD
GST-E2FA
AB-GST
EA-POD
B
BRCA1-N/RBR-C
RBR-N/SCR-C
BRCA1-N/SCR-C

Figure 6

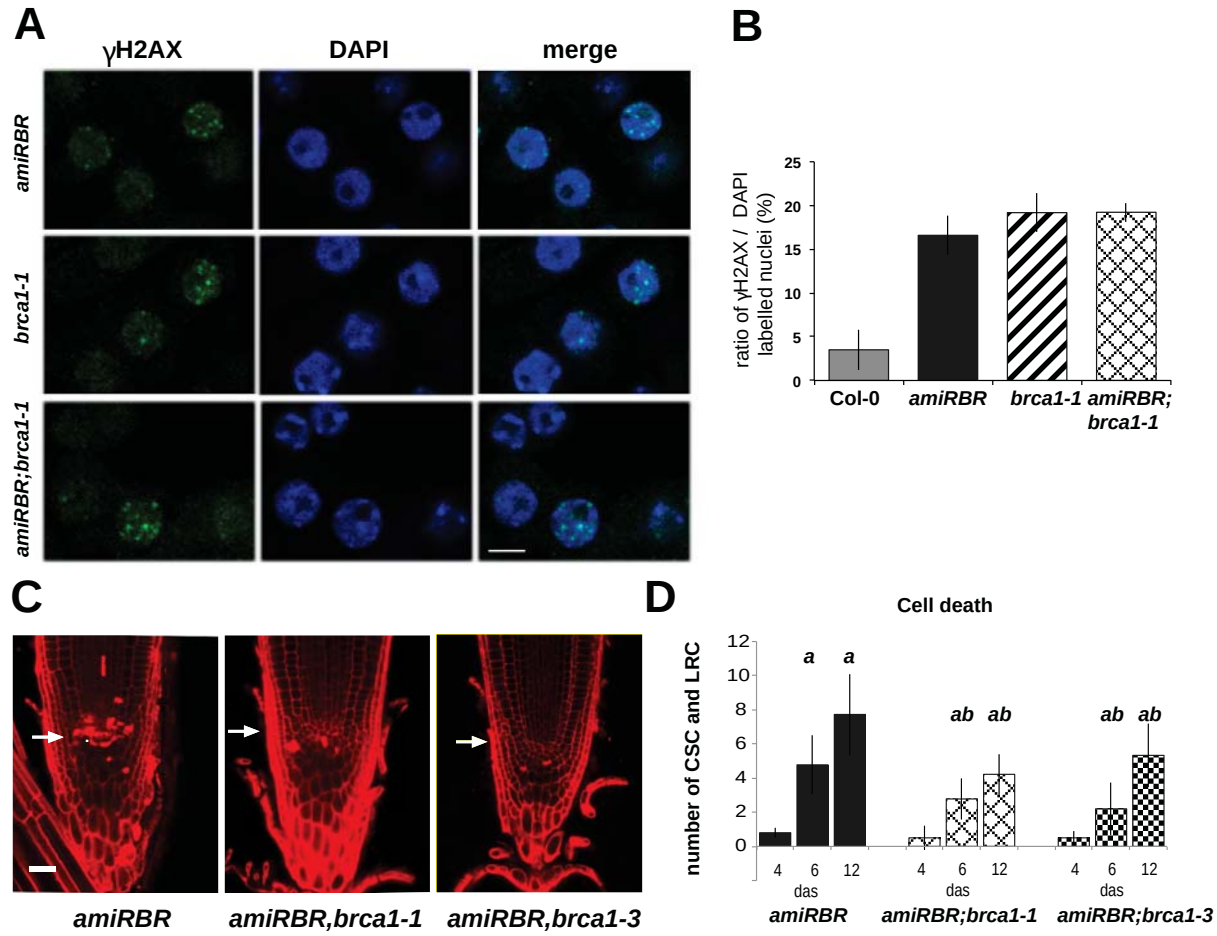
A
γH2AX
DAPI
merge
amiRBR
brca1-1
amiRBR;brca1-1
B
ratio of γH2AX / DAPI labelled nuclei (%)
25
20
15
10
5
0
Col-0
amiRBR
brca1-1
amiRBR; brca1-1
C
amiRBR
amiRBR,brca1-1
amiRBR,brca1-3
D
Cell death
number of CSC and LRC
12
10
8
6
4
2
0
a
a
ab
ab
ab
ab
4
6
12
das
amiRBR
amiRBR;brca1-1
amiRBR;brca1-3

Figure 7

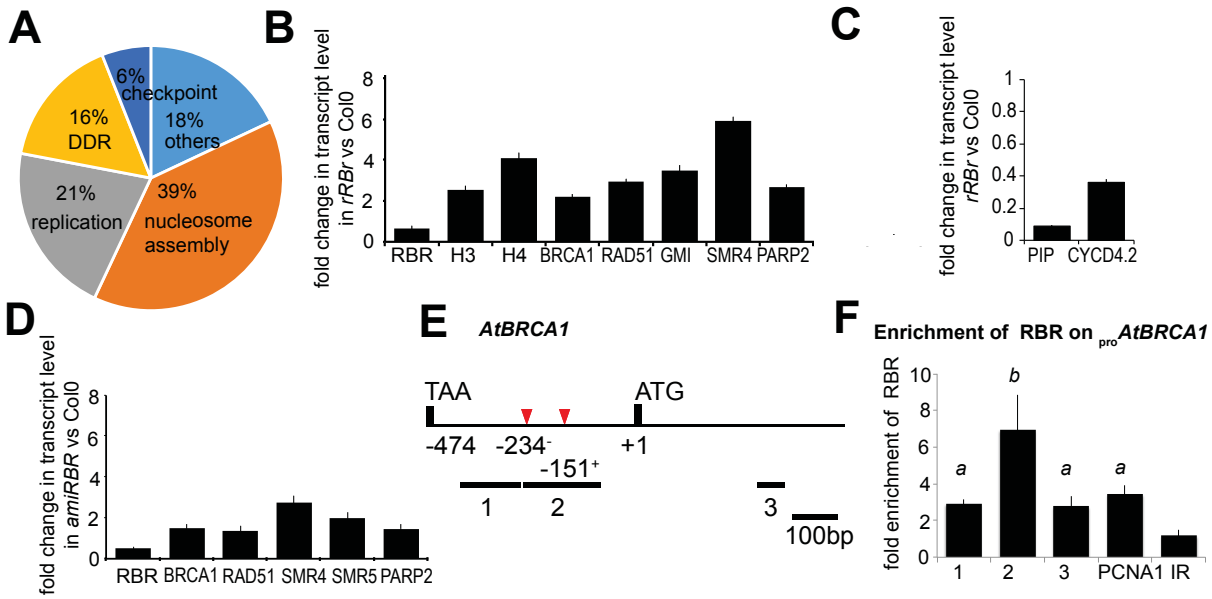
A
6%
checkpoint
18%
others
16%
DDR
21%
replication
39%
nucleosome
assembly
B
fold change in transcript level
in rRBr vs Col0
RBR H3 H4 BRCA1 RAD51 GMI SMR4 PARP2
C
fold change in transcript level
rRBr vs Col0
PIP CYCD4.2
D
fold change in transcript level
in amiRBR vs Col0
RBR BRCA1 RAD51 SMR4 SMR5 PARP2
E
AtBRCA1
TAA
ATG
-474
-234
-151
+1
1
2
3
100bp
F
Enrichment of RBR on proAtBRCA1
fold enrichment of RBR
a
b
a
a
1 2 3 PCNA1 IR

Figure 8

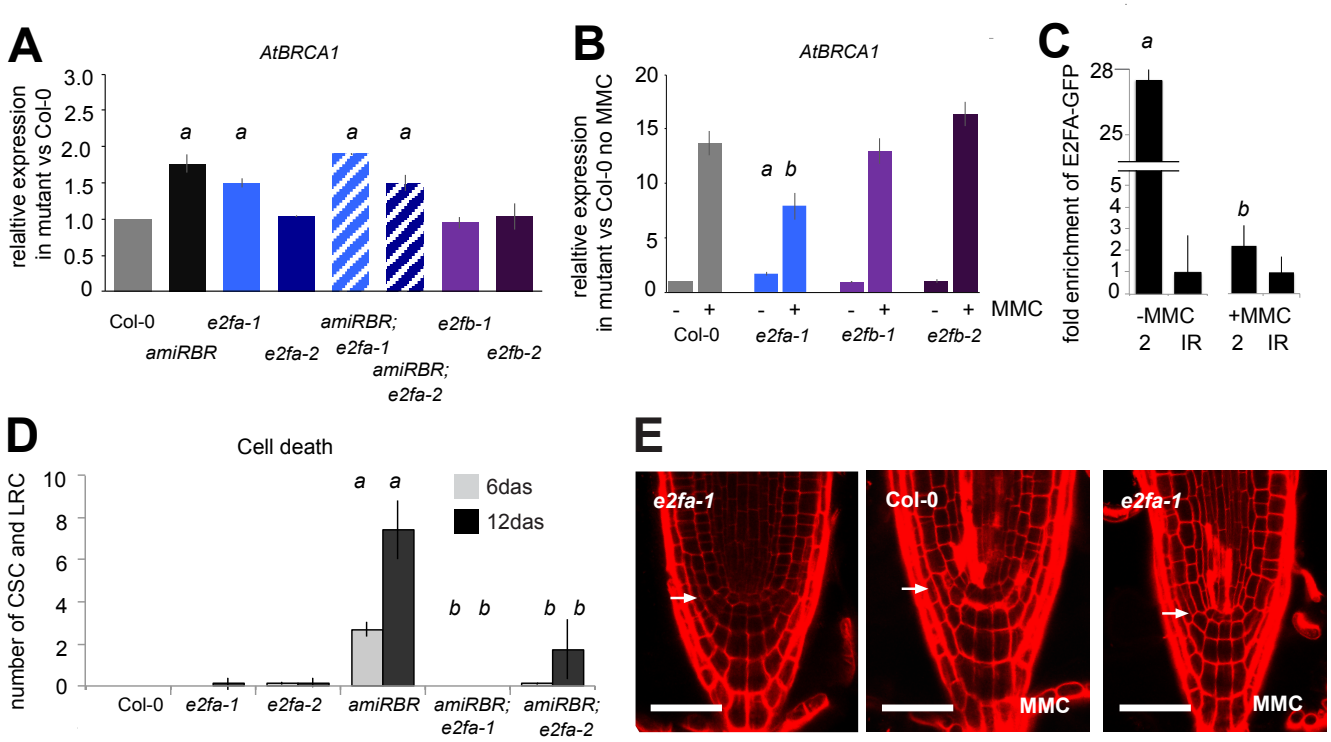
A
AtBRCA1
relative expression in mutant vs Col-0
3.0
2.5
2.0
1.5
1.0
0.5
0
a a a a
Col-0
amiRBR
e2fa-1
e2fa-2
amiRBR; e2fa-1
amiRBR; e2fa-2
e2fb-1
e2fb-2
B
AtBRCA1
relative expression in mutant vs Col-0 no MMC
20
15
10
5
0
a b
- + - + - + - +
MMC
Col-0
e2fa-1
e2fb-1
e2fb-2
C
fold enrichment of E2FA-GFP
a
28
25
5
4
3
2
1
0
b
-MMC
+MMC
2 IR 2 IR
D
Cell death
number of CSC and LRC
10
8
6
4
2
0
a a
b b b b
6das
12das
Col-0
e2fa-1
e2fa-2
amiRBR
amiRBR; e2fa-1
amiRBR; e2fa-2
E
e2fa-1
Col-0
MMC
e2fa-1
MMC

Figure 9

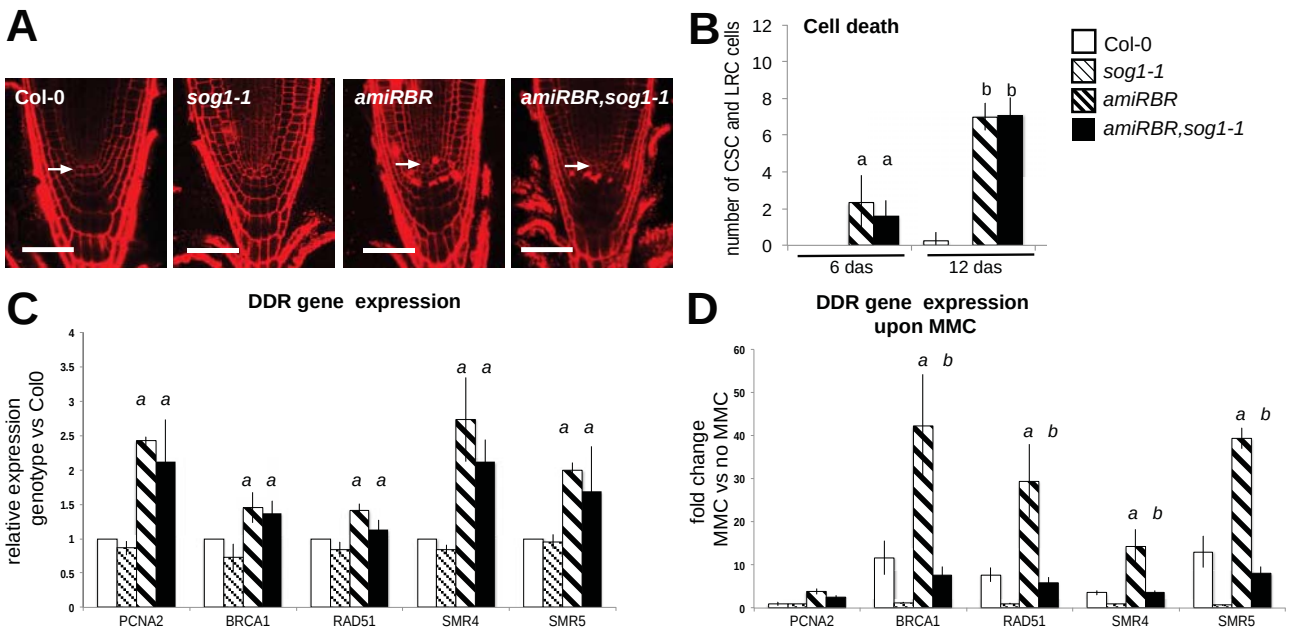
A
Col-0
sog1-1
amiRBR
amiRBR,sog1-1
B
Cell death
number of CSC and LRC cells
12
10
8
6
4
2
0
a a
b b
6 das
12 das
Col-0
sog1-1
amiRBR
amiRBR,sog1-1
C
DDR gene expression
relative expression genotype vs Col0
4
3.5
3
2.5
2
1.5
1
0.5
0
a a
a a
a a
a a
a a
PCNA2
BRCA1
RAD51
SMR4
SMR5
D
DDR gene expression upon MMC
fold change MMC vs no MMC
60
50
40
30
20
10
0
a b
a b
a b
a b
a b
PCNA2
BRCA1
RAD51
SMR4
SMR5

Figure EV1

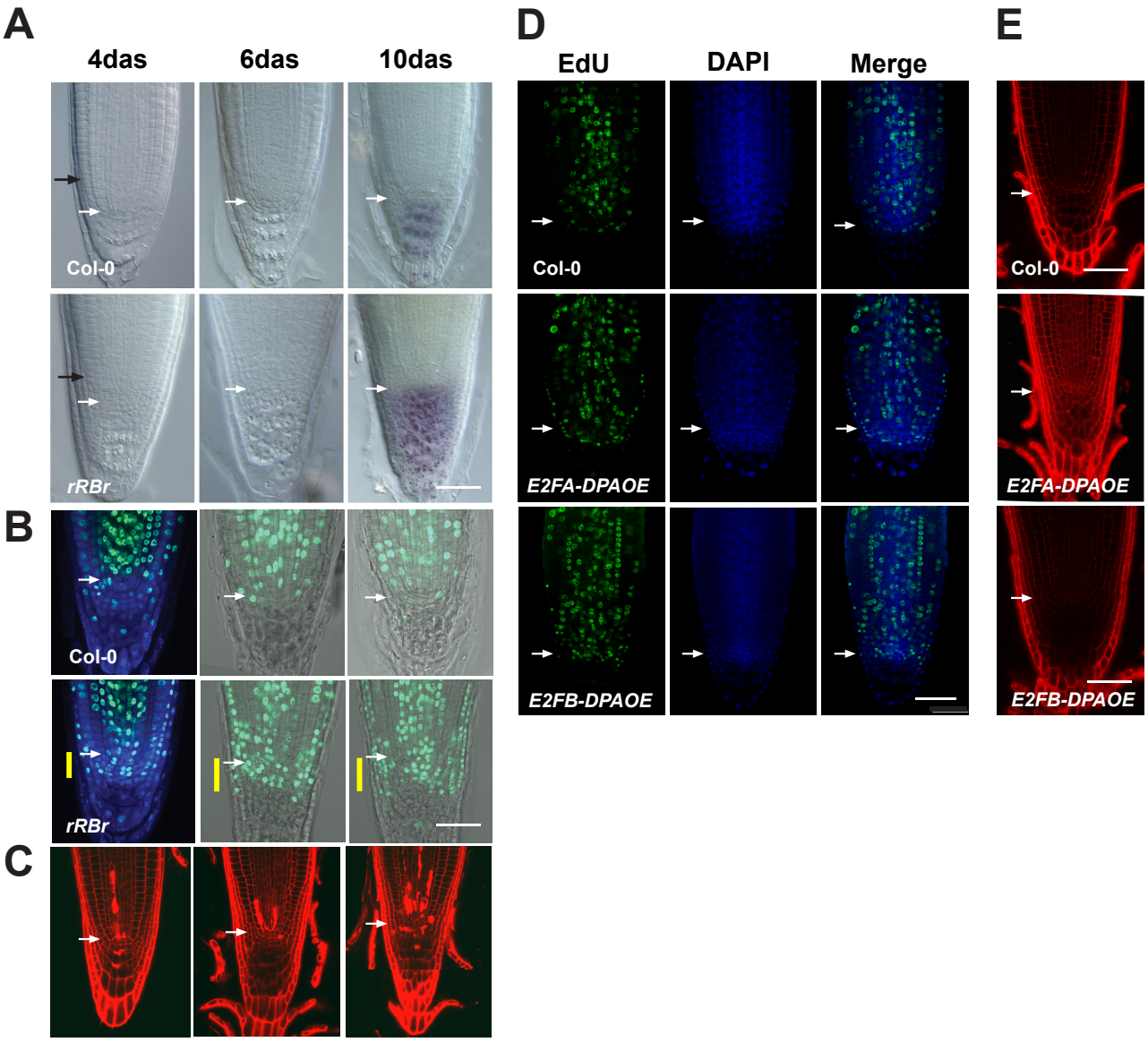
A
4das
6das
10das
Col-0
rRBr
B
Col-0
rRBr
C
D
EdU
DAPI
Merge
Col-0
E2FA-DPAOE
E2FB-DPAOE
E
Col-0
E2FA-DPAOE
E2FB-DPAOE

Figure EV2

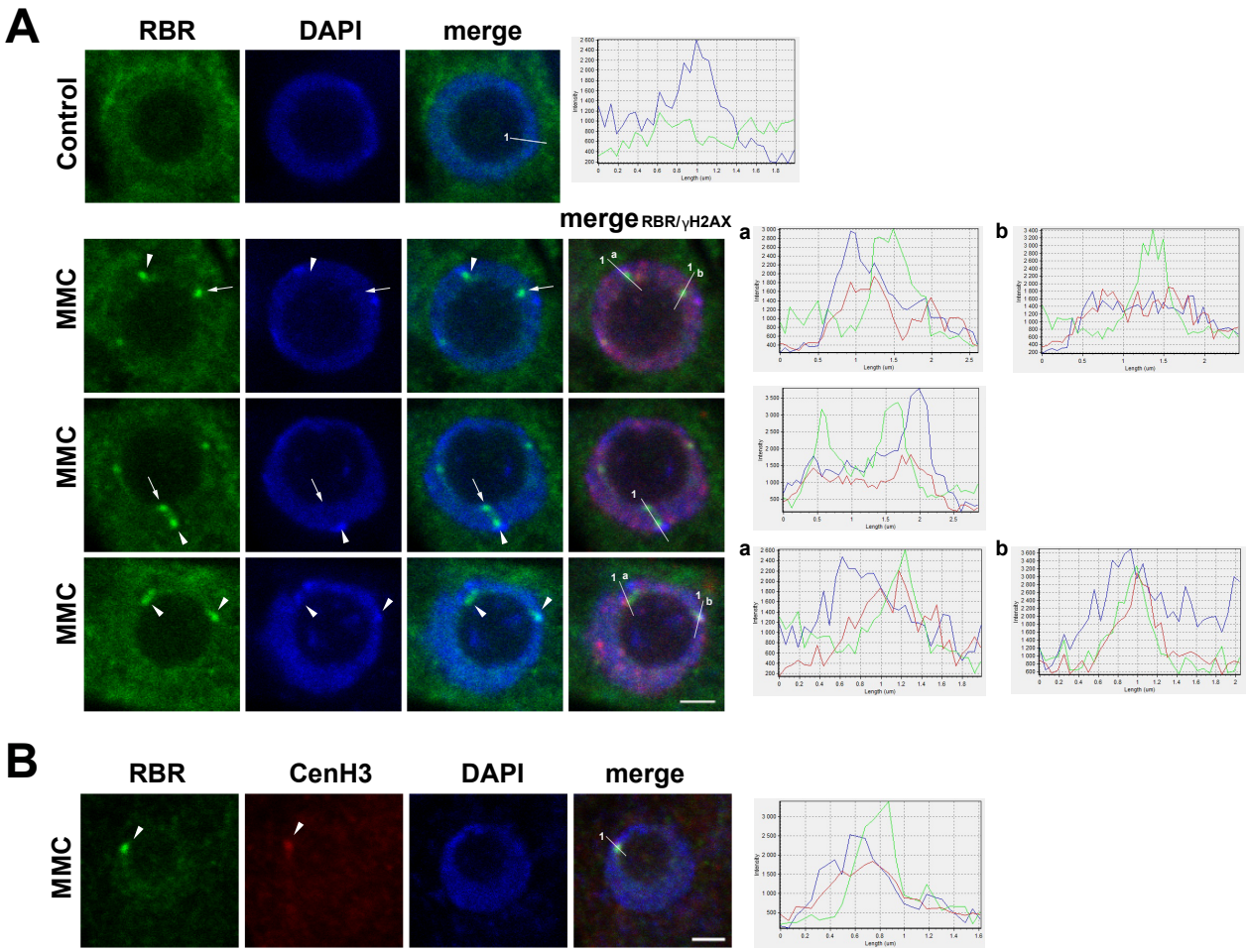
A
RBR
DAPI
merge
Control
merge RBR/γH2AX
MMC
MMC
MMC
a
b
a
b
B
RBR
CenH3
DAPI
merge
MMC

Figure EV3

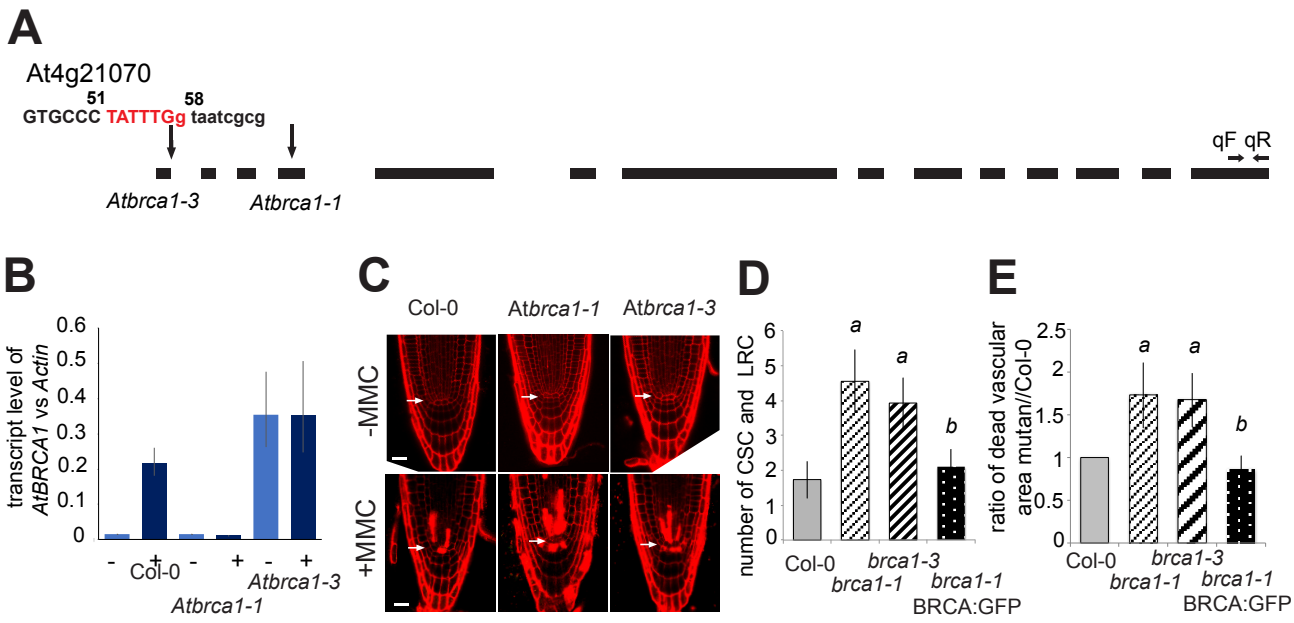
A
At4g21070
51
58
GTGCCC TATTTGg taatcgcg
qF qR
Atbrca1-3
Atbrca1-1
B
transcript level of AtBRCA1 vs Actin
0.6
0.5
0.4
0.3
0.2
0.1
0
- + - + - +
Col-0
Atbrca1-3
Atbrca1-1
C
Col-0
Atbrca1-1
Atbrca1-3
-MMC
+MMC
D
number of CSC and LRC
6
5
4
3
2
1
0
a
a
b
Col-0
brca1-3
brca1-1
brca1-1
BRCA:GFP
E
ratio of dead vascular area mutan//Col-0
2.5
2
1.5
1
0.5
0
a
a
b
Col-0
brca1-3
brca1-1
brca1-1
BRCA:GFP

Figure EV4

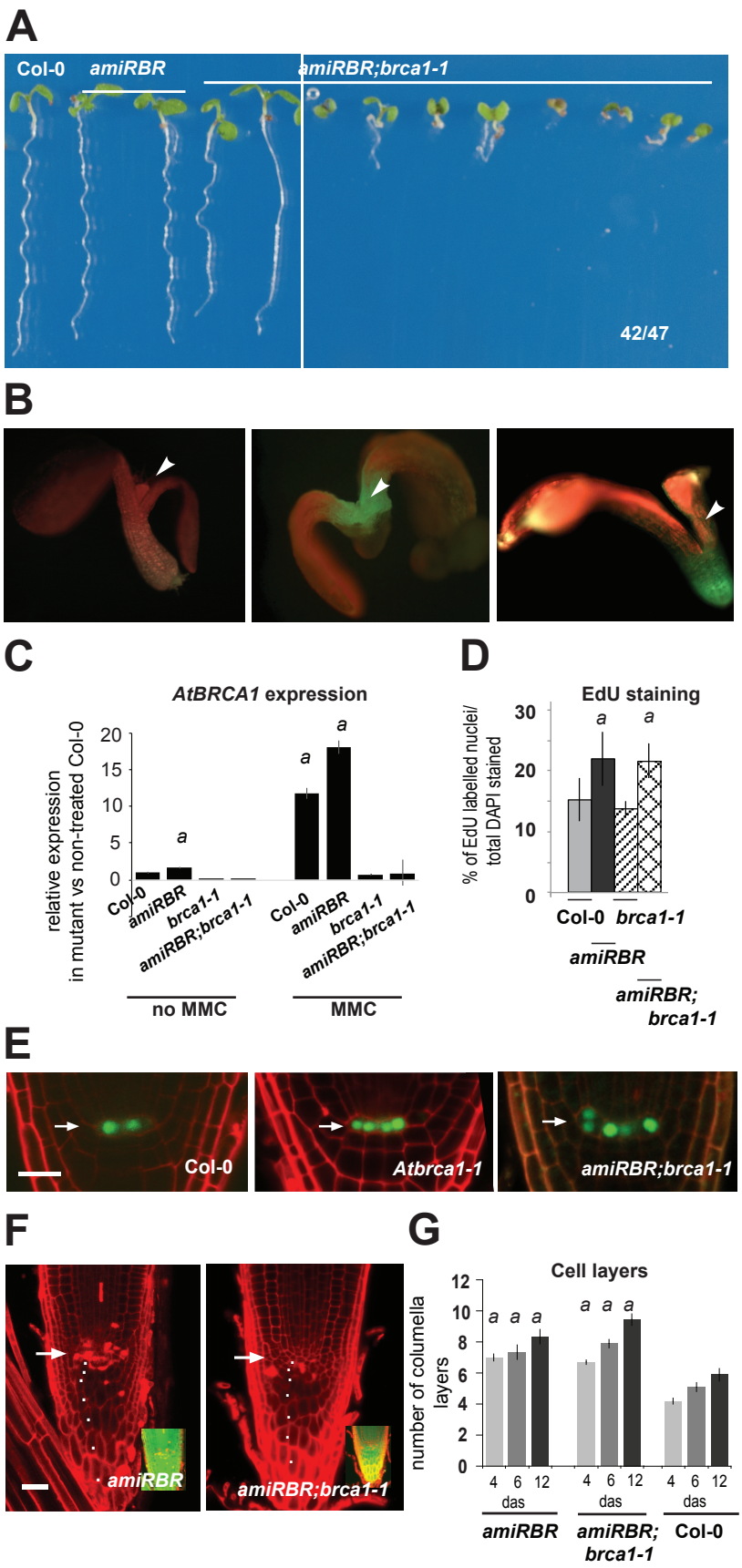
A
Col-0
amiRBR
amiRBR;brca1-1
42/47
B
C
AtBRCA1 expression
relative expression in mutant vs non-treated Col-0
20
15
10
5
0
a
a
a
Col-0
amiRBR
brca1-1
amiRBR;brca1-1
Col-0
amiRBR
brca1-1
amiRBR;brca1-1
no MMC
MMC
D
EdU staining
% of EdU labelled nuclei/ total DAPI stained
30
20
10
0
a
a
Col-0
brca1-1
amiRBR
amiRBR; brca1-1
E
Col-0
Atbrca1-1
amiRBR;brca1-1
F
amiRBR
amiRBR;brca1-1
G
Cell layers
number of columella layers
12
10
8
6
4
2
0
a a a
a a a
4 6 12
das
4 6 12
das
4 6 12
das
amiRBR
amiRBR; brca1-1
Col-0

Figure EV5

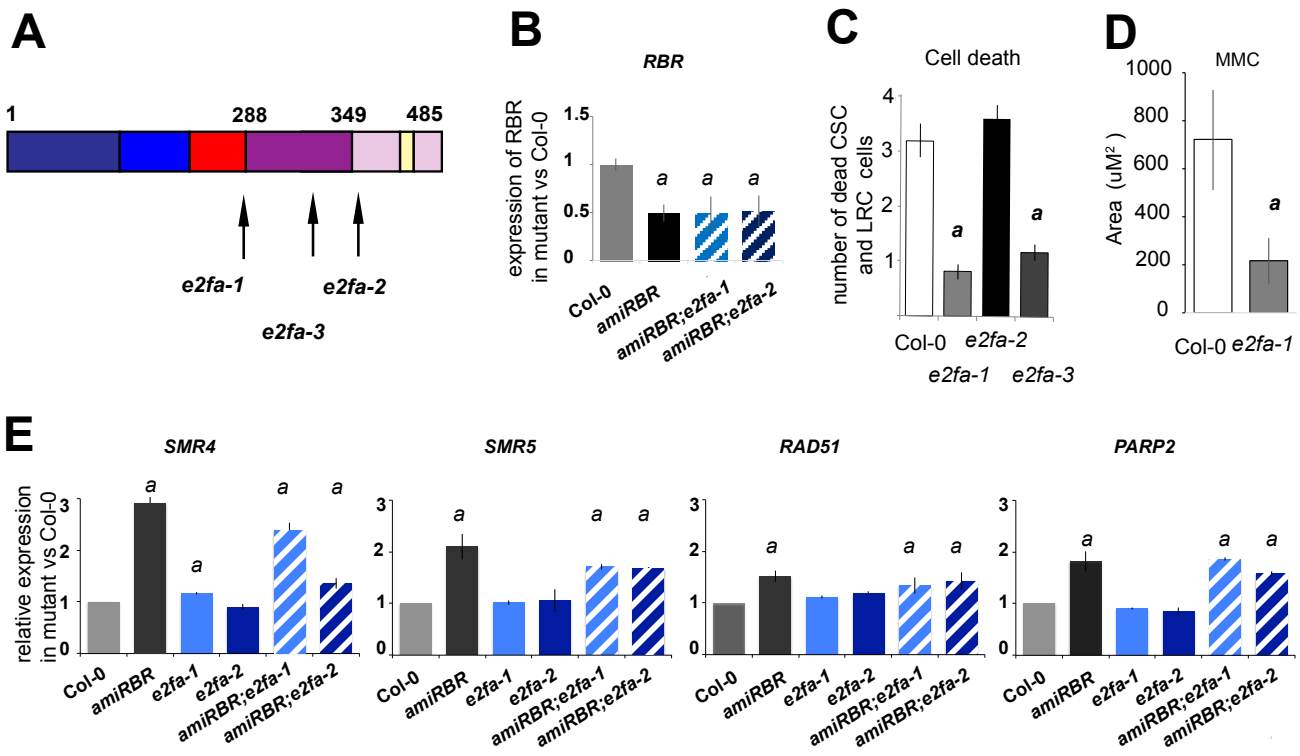
A
1
288
349
485
e2fa-1
e2fa-2
e2fa-3
B
RBR
expression of RBR in mutant vs Col-0
1.5
1
0.5
0
a
a
a
Col-0
amiRBR
amiRBR;e2fa-1
amiRBR;e2fa-2
C
Cell death
number of dead CSC and LRC cells
4
3
2
1
a
a
Col-0
e2fa-2
e2fa-1
e2fa-3
D
MMC
Area (uM²)
1000
800
600
400
200
0
a
Col-0
e2fa-1
E
SMR4
SMR5
RAD51
PARP2
relative expression in mutant vs Col-0
3
2
1
0
a
Col-0
amiRBR
e2fa-1
e2fa-2
amiRBR;e2fa-1
amiRBR;e2fa-2

Figure EV6

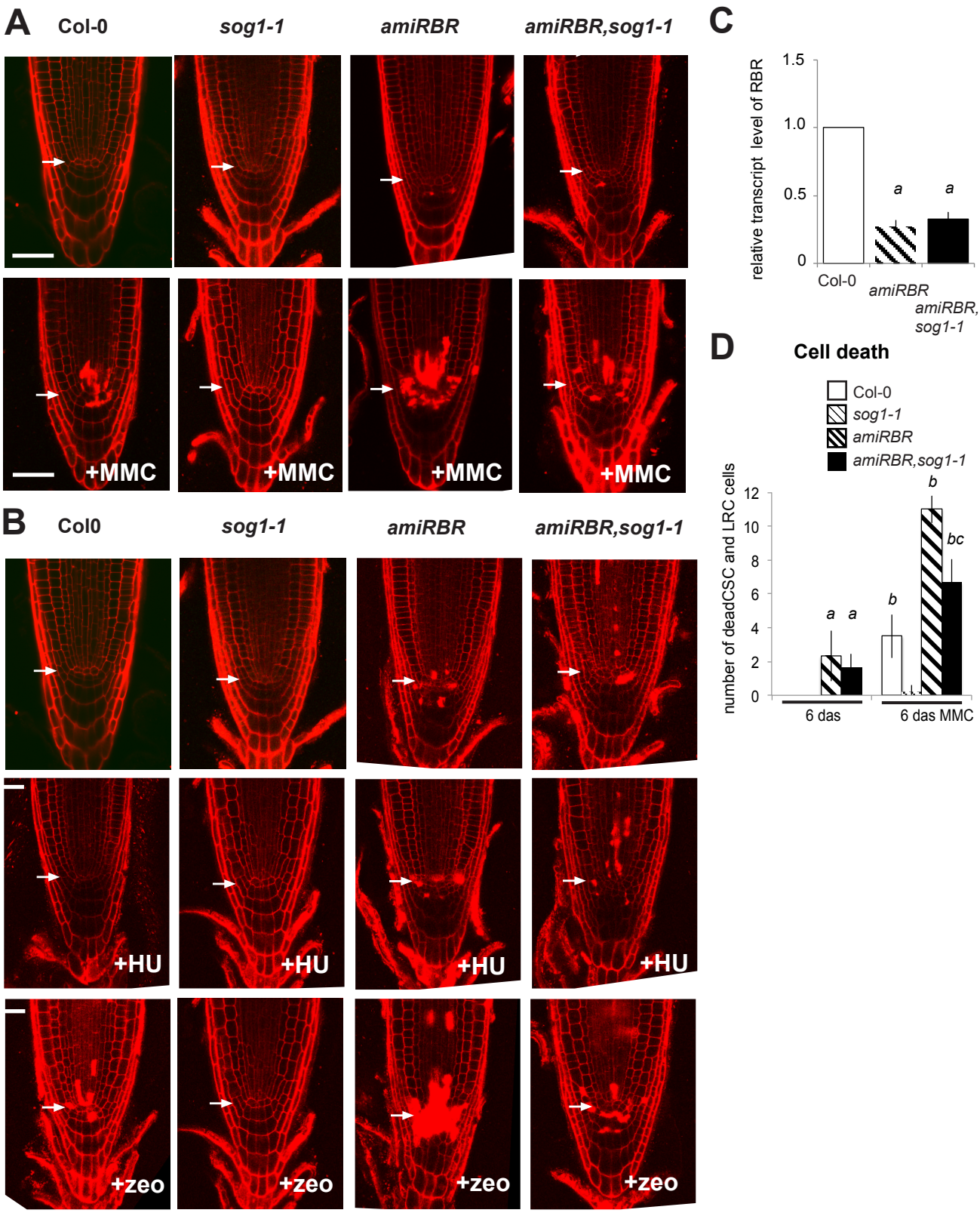
A
Col-0
sog1-1
amiRBR
amiRBR,sog1-1
+MMC
B
Col0
sog1-1
amiRBR
amiRBR,sog1-1
+HU
+zeo
C
relative transcript level of RBR
1.5
1.0
0.5
0
a
a
Col-0
amiRBR
amiRBR,
sog1-1
D
Cell death
Col-0
sog1-1
amiRBR
amiRBR,sog1-1
number of deadCSC and LRC cells
12
10
8
6
4
2
0
a
a
b
b
bc
6 das
6 das MMC

Table S1 –List of differentially expressed genes in root-tip comparing transcriptome of *rRBr* and Col-0

											sog1-	*atm-2*	*E2F* motif	*CYCD3 OE*	*E2Fa* OE	inducible		RBR	RNAi				
	Annotation	Locus	FC		adj. p-value											3hai	6hai	12ha	24hai	3hai	6hai	12hai	24hai
	Upregulated		(≥1.4)			ATEDII										up	up	up	up	down	down	down	down
1	Histone superfamily protein	At1g09200	1.62	11.74	1.53E-05		x						x	xxx	#	0	0	7	9	0	0	0	0
2	Acetyl-CoA carboxylase 2 (ACC2)	At1g36180	3.12	5.68	2.44E-05	C		x								0	0	0	0	0	0	0	0
3	Histone H2A protein (HTA13)	At3g20670	1.93	11.11	2.44E-05		x							xxx	#	0	0	8	9	0	0	0	0
4	Unknown protein	At5g05180	5.66	6.15	2.44E-05									xxx	#	0	0	0	5	0	0	0	0
5	Chromatin remodeling factor CHR31)	At1g05490	1.5	3.96	4.74E-05								x		#	0	0	0	0	0	0	0	0
6	Zinc finger (C3HC4-type RING finger) family protein	At5g60250	4.04	5.15	4.76E-05	C		x			x	xx	x	xxx	#	0	0	0	0	0	0	0	0
7	Histone superfamily protein	At3g53650	1.87	8.33	1.46E-04	AC	x	x					x	xxx	#	0	0	9	9	0	0	0	0
8	Histone2A protein (HTA1)	At5g54640	1.94	9.26	1.46E-04	A	x							xxx	#	0	0	6	0	0	0	0	0
9	Histone 2B protein (HTB9)	At3g45980	1.49	12.12	1.46E-04	A	x						x	xxx	#	0	0	2	9	0	0	0	0
10	Histone superfamily protein	At2g37470	1.48	9.25	1.48E-04	AC	x							xxx		0	0	5	9	0	0	0	0
11	Histone superfamily protein	At3g27360	1.63	10.57	1.84E-04		x							xxx		0	0	7	9	0	0	0	0
12	Histone superfamily protein	At1g07820	1.51	10.99	2.12E-04		x						x	xxx	#	0	0	2	6	0	0	0	0
13	Homolog of Drosophila timeless (ATIM)	At5g52910	1.56	6.85	2.35E-04				x				x	xxx	#	0	0	9	9	0	0	0	0
14	Unknown protein	At3g48490	1.99	7.24	2.44E-04								x	xxx	#	0	0	9	9	0	0	0	0
15	Siamese-related, SMR4	At5g02220	4.3	7.22	2.44E-04	C		x			x	xx	x	xxx	#	0	0	1	0	0	0	0	0
16	Histone H2A protein (HTA2)	At4g27230	1.74	10.46	2.64E-04	A	x							xxx	#	0	0	7	6	0	0	0	0
17	Siamese-related, SMR6	At5g40460	1.57	6.26	2.64E-04								x		#	0	0	0	0	0	0	0	0

18	Histone superfamily protein	At5g59690	1.55	13.04	3.48E-04		x						x	xxx	#	0	0	3	9	0	0	0	0
19	Histone H2A protein (HTA6)	At5g59870	1.4	12	3.48E-04		x						x	xxx	#	0	0	5	9	0	0	0	0
20	Histone H1.1 protein	At1g06760	1.52	11	4.91E-04	A	x									0	0	0	9	0	0	0	0
21	Homolog to breast cancer susceptibility gene 1 (BRCA1)	At4g21070	2.04	6.59	5.23E-04	C		x			x	xx	x	xxx	#	0	0	8	7	0	0	0	0
22	Histone 2B protein (HTB1)	At1g07790	1.56	10.73	5.85E-04	A	x									0	0	7	8	0	0	0	0
23	Histone superfamily protein	At5g10400	1.53	10.63	6.45E-04		x						x	xxx	#	0	0	7	9	0	0	0	0
24	Histone superfamily protein	At2g28720	2.71	7.63	6.68E-04		x									0	0	7	8	0	0	0	0
25	Histone H2A protein (HTA11)	At3g54560	1.56	10.72	6.86E-04		x						x	xxx	#	0	0	0	9	0	0	0	0
26	Kip-related protein (KRP3)	At5g48820	1.68	7.31	7.21E-04				x	x					#	0	0	0	3	0	0	0	0
27	Histone superfamily protein	At3g09480	1.75	8.54	7.85E-04	AC	x									0	0	8	7	0	0	0	0
28	Adenine nucleotide alpha hydrolases-like superfamily protein	At1g44760	1.68	7.87	8.39E-04											0	0	0	0	0	0	0	0
29	Histone superfamily protein	At5g10980	1.45	12.32	1.02E-03	A	x									0	0	0	1	0	0	0	0
30	Histone superfamily protein	At5g65360	1.39	11.29	1.02E-03		x					xx	x	xxx	#	0	0	4	9	0	0	0	0
31	Homolog of yeast RAD51	At5g20850	1.42	6.95	1.05E-03	C		x			x	xx			#	0	0	6	0	0	0	0	0
32	Histone superfamily protein	At5g02570	1.67	6.54	1.19E-03		x									0	0	3	0	0	0	0	0
33	High mobility group B (HMGB6)	At5g23420	1.58	8.08	1.55E-03				x				x	xxx	#	0	0	7	9	0	0	0	0
34	WRKY DNA-binding protein 21 (WRKY21)	At2g30590	1.54	7.47	1.61E-03										#	0	0	0	0	0	0	0	0

35	Minichromosome maintenance complex (MCM7), Prolifera	At4g02060	1.54	9.21	1.82E-03				x				x	xxx	#	0	0	9	9	0	0	0	0
36	Histone superfamily protein	At3g53730	1.41	11.73	1.91E-03	A	x						x	xxx	#	0	0	7	9	0	0	0	0
37	Histone superfamily protein	At4g40040	1.66	12.06	2.00E-03	A	x						x	xxx		0	0	0	0	0	0	0	0
38	DNA dependent nuclear poly (ADP-ribose) polymerase (PARP2)	At4g02390	1.68	6.68	2.09E-03	C		x			x	xx			#	0	0	2	1	0	0	0	1
39	Histone 3 11 (HTR11)	At5g65350	2.25	5.65	2.50E-03		x						x			0	0	0	0	0	0	0	0
40	Protein kinase superfamily protein	At4g35030	1.57	6.21	2.60E-03							xx	x			0	0	0	0	0	0	0	3
41	Unknown protein	At1g35780	1.49	9.18	2.60E-03								x	xxx		0	0	0	0	0	0	0	0
42	Unknown protein	At5g54970	1.49	10.26	2.71E-03	B			x				x	xxx	#	0	0	9	9	0	0	0	0
43	Catalytic subunit of the DNA polymerase alpha, putative (ICU2)	At5g67100	1.5	7.42	3.29E-03			x	x	x			x	xxx	#	0	0	0	9	0	0	0	0
44	Histone superfamily protein	At5g50930	1.44	5.97	3.47E-03									xxx	#	0	0	6	6	0	0	0	0
45	AT hook motif DNA-binding family protein (AHP1)	At2g33620	1.46	7.2	3.47E-03											0	0	0	0	0	0	0	0
46	Ribonucleotide reductase (RNR) small subunit gene (TSO2)	At3g27060	1.5	10.55	3.50E-03	B		x	x	x		xx	x	xxx	#	0	0	8	9	0	0	0	0
47	D-mannose binding lectin protein	At5g03700	1.4	7.47	3.50E-03								x		#	0	0	0	0	0	0	7	4
48	TESMIN/TSO1-like CXC 2 (TCX2)	At4g14770	1.99	7.72	3.50E-03				x				x	xxx	#	0	0	8	9	0	0	0	0
49	Structural Maintenance of Chromosomes 6A (SMC6A)	At5g07660	1.78	4.53	3.50E-03			x	x				x		#	0	0	7	0	0	0	0	0
50	Transducin/WD40 repeat-like superfamily protein	At3g27640	1.37	7.21	3.50E-03				x				x		#	0	0	7	7	0	0	0	0

51	Member of TRFL family 2 (TRFL10)	At5g03780	1.44	5.67	3.58E-03	C		x			x	xx			#	0	0	0	0	0	0	0	0
52	Glycoside Hydrolase Family 16 (XTH28)	At1g14720	1.61	7.01	4.05E-03							xx	x			0	0	0	0	0	0	0	0
53	Actin-binding formin homology 2	At3g07540	1.73	5.51	4.08E-03											0	0	0	0	0	0	8	4
54	Histone superfamily protein	At3g45930	1.49	10.9	4.09E-03		x						x	xxx	#	0	0	9	9	0	0	0	0
55	Proliferating Cell Nuclear Antigen 2 (PCNA2)	At2g29570	1.41	10.81	4.43E-03	B			x				x	xxx	#	0	0	9	9	0	0	0	0
56	Histone 2B protein (HTB2)	At5g22880	1.66	9.33	4.43E-03		x						x	xxx	#	0	0	6	9	0	0	0	0
57	ATP binding microtubule motor family protein	At3g63480	1.6	6.39	4.61E-03				x						#	0	0	7	0	0	0	0	0
58	Histone 4	At2g28740	1.39	9.88	4.61E-03		x						x		#	0	0	6	8	0	0	0	0
59	Cytochrome P450 superfamily protein	At1g73340	1.88	7.63	4.77E-03											0	0	0	0	0	0	0	0
60	NAC domain containing protein 103 (NAC103)	At5g64060	1.72	5.36	5.02E-03	C		x			x	xx		xxx	#	0	0	0	0	0	0	0	0
61	Unknown protein	At4g28310	1.41	9.32	5.34E-03	B			x				x	xxx	#	0	0	9	9	0	0	0	0
62	Agenet domain-containing protein	At1g26540	1.65	4.85	5.68E-03								x		#	0	0	5	3	0	0	0	0
63	Histone superfamily protein	At5g10390	1.43	9.96	5.78E-03		x						x	xxx	#	0	0	7	9	0	0	0	0
64	Cytokinin response factor (CRF6)	At3g61630	1.52	4.59	5.78E-03							xx	x			0	0	3	0	0	0	4	7
65	DNA polymerase alpha 2 (POLA2)	At1g67630	1.55	7.69	5.78E-03			x	x	x				xxx	#	0	0	9	9	0	0	0	0
66	Chromatin remodeling factor17 (CHR17)	At5g18620	1.54	9.4	5.78E-03				x				x	xxx	#	0	0	5	9	0	0	0	0
67	Cystatin/monellin family protein	At5g05110	1.76	6.25	5.78E-03									xxx		0	0	0	0	0	0	0	0
68	GATA transcription factor (GATA5)	At5g66320	1.53	6.22	5.78E-03											0	0	5	9	0	0	0	0

69	Homolog of homologous -pairing protein2 hop2 (AHP2)	At1g13330	1.97	4.94	6.18E-03	C		x	x			xx		xxx	#	0	0	6	0	0	0	0	0
70	NAC domain protein (BRN2)	At4g10350	2.52	7.65	6.27E-03								x			0	0	0	0	0	0	0	0
71	Homolog of the human centromeric protein C (CENP-C)	At1g15660	1.48	8.87	6.58E-03				x	x			x	xxx	#	0	0	1	7	0	0	0	0
72	Protein of unknown function (DUF239)	At1g70550	1.68	7.4	6.72E-03									xxx		0	0	0	0	2	0	0	0
73	Gamma-irradiation and mitomycinin C induced 1 (GMI1)	At5g24280	2.09	5.28	7.10E-03	C		x			x	xx		xxx	#	0	0	3	0	0	0	0	0
74	Unknown protein	At3g01860	1.42	5.23	7.25E-03								x			0	0	0	0	0	0	0	0
75	Senescence/dehydration-associated protein-related	At4g35985	1.47	6.5	7.25E-03								x			0	0	1	0	0	0	1	0
76	High mobility group A (HMGA)	At1g14900	1.5	9.43	7.53E-03		x						x	xxx		0	0	3	0	0	0	0	0
77	F-box family protein	At4g35930	1.49	6.42	8.55E-03								x		#	0	0	0	3	0	0	0	0
78	TRAM, LAG1 and CLN8 (TLC) lipid-sensing domain containing protein	At1g21790	1.5	6.68	8.56E-03											0	0	0	0	0	0	0	4
79	WRKY transcription factor (WRKY48)	At5g49520	1.76	4.66	8.56E-03								x		#	0	0	0	0	0	0	8	6
80	Replicon Protein A2 (RPA2)	At2g24490	1.45	9.24	8.63E-03	B			x	x			x	xxx	#	0	0	9	9	0	0	0	0
81	DNA primase, large subunit family	At1g67320	1.43	7.96	9.31E-03				x	x			x	xxx	#	0	0	6	9	0	0	0	0
82	Kip-related protein (KRP5)	At3g24810	1.6	6	9.31E-03					x						0	0	0	6	0	0	0	0
														46					58			7	
	Down-regulated																						
1	Phosphatidylinositol 3- and 4-kinase	At5g24240	-4.31	5.89	2.57E-06								x	xxx		0	0	0	0	0	0	0	0

2	HSP20-like chaperones superfamily protein	At5g47600	-3.93	6.15	3.58E-03											0	0	0	0	0	0	0	0
3	ARF GTPase family (ARFB1B)	At5g17060	-3.71	7.06	2.36E-08											0	0	0	0	0	0	0	0
4	Unknown protein	At5g15725	-3.65	5.21	1.46E-04											0	0	0	0	0	0	0	0
5	TRICHOME BIREFRINGENCE-LIKE (TBL6)	At3g62390	-3.09	6.34	1.53E-05											0	0	0	0	0	0	0	6
6	Retinoblastoma-related protein (RBR)	At3g12280	-2.26	7.86	7.85E-06				x	x			x	xxx	#	0	0	0	0	0	4	9	7
7	emp24/gp25L/p24 family/GOLD family protein	At3g10780	-2.22	5	6.92E-03								x			0	0	0	0	0	0	0	0
8	QUA-QUINE STARCH (QQS)	At3g30720	-1.92	4.77	2.64E-04											0	4	0	1	0	0	3	0
9	Putative receptor serine/threonine kinase PR5K (PR5K)	At5g38280	-1.8	5.49	1.37E-03											0	0	0	0	0	0	0	0
10	D-type cyclin CYCD4 (CYCD4;1)	At5g65420	-1.69	5.63	4.61E-03					x						0	0	1	0	0	0	0	0
11	WNK protein kinases (WNK7)	At1g49160	-1.61	5.17	5.78E-03											0	0	0	0	0	0	0	0
12	MRP subfamily (MRP11)	At2g07680	-1.51	6.29	1.19E-03											0	0	0	0	0	0	0	0
13	BRGs (BOI-related gene) involved in resistance to Botrytis cinerea (BRG2)	At1g79110	-1.48	4.21	6.94E-03								x		#	0	0	2	8	0	0	0	0
14	D-type cyclin CYCD4 (CYCD4;2)	At5g10440	-1.48	4.63	8.39E-04					x						0	0	0	0	0	0	0	0
15	Oxidoreductase activity, acting on the CH-CH group of donors	At1g18180	-1.46	7.08	3.47E-03											0	0	0	0	0	0	1	0
16	RNA-binding KH domain-containing protein	At3g32940	-1.46	6.85	3.58E-03											0	0	0	0	0	0	0	0

17	Purple acid phosphatase 27 (PAP27)	At5g50400	-1.45	7.35	4.77E-03											0	0	0	0	0	0	0	0
							32	14	19	6	8	14	53	48	56			2				3	

APPENDIX

Table of Contents

Supplementary Methods

Immuno-labelling and fluorescence microscopy

Primary and secondary antibodies used for immune-fluorescence labelling were diluted as follows: anti-γ-H2AX (Friesner *et al*, 2005, Amiard *et al*, 2010, kindly provided by Ch. I. White, Clermont Université, France); 1:600 for Alexa Fluor 488 and 1:1000 for Alexa Fluor 594 secondary antibody, anti-RBR1 (Agrisera) 1:7000, mouse and rabbit anti-GFP (Abcam) 1:250, 1:3000, respectively and anti-CenH3 (Abcam) 1:800. Alexa Fluor 488, Alexa Fluor 594, Alexa Fluor 647- conjugated anti-mouse, anti-rabbit and anti-chicken antibodies (Jackson ImmunoResearch Laboratories) were diluted 1:600, 1:800, 1:700, respectively. Chromatin was stained by DAPI.

For fluorescence microscopy Olympus IX-81 FV-1000 confocal imaging system was used with oil immersion objective 100x/1.45, and dry objective 40x/0.95 was used; DAPI excitation (ex) was 405 nm, and emission (em) was at 425-460 nm, Alexa488 ex 473 nm, em 485-545 nm; Alexa 594 ex 559 nm, em 575-640 nm; Alexa 647 ex 635 nm, em 655-755 nm. Laser scanning was performed using the sequential multi-track mode to avoid bleed-through. Chromatic shift and aberration of the optical system was determined and corrected with FV10 ASW2.0 (Olympus, Tokyo, Japan) software using TetraSpeck 0.21 μm beads

(Invitrogen) as fiducial markers. Images were analysed by FV10 ASW2.0 and prepared in Adobe Photoshop CS4 and Adobe Illustrator CS4. Counting of immune-labelled nuclei and foci was performed in Adobe Photoshop CS6 extended using objects counting functions.

EdU staining

5-Ethynyl-2´-deoxyuridine (EdU) labelling was performed in whole mount preparation of root tips. EdU pulse was applied in dilution of 1:1000 and seedlings incubated in dark for 1h. Seedlings were fixed in 3.7 % formaldehyde in MTSB, pH 6.9 for 1h. Samples were then washed in MTSB, treated with 0.5 % Triton in PBS for 15 min, washed and incubated for 40 min in Click-IT reaction mixture (Molecular Probes, Eugene, OR, USA).

Generating functional AtBRCA1 constructs

The full-length genomic fragment (from ATG to stop codon, 4457bp) was used to generate the GFP and 10xmyc markers labelled AtBRCA1 protein. To express the AtBRCA1-GFP protein the promoter region (-383 to -1) was used, while for overexpression, the GVX1090 promoter. The At*brca1-1* mutant was used as a genetic background for transformation. Several independent transformants were recovered and analysed functionally. The AtBRCA1-GFP construct was detectable via confocal microscopy after MMC induction, while Western blot analysis was carried out to study the presence of the AtBRCA1-10xmyc protein after β-estradiol induction (24 hrs, 5 µM β–estradiol, Appendix Fig S1).

Interaction of *in vitro* translated proteins

To test whether AtBRCA1 and RBR proteins interact, we translated them *in vitro* in wheat germ extract and used the translated E2FA and E2FB as positive controls. RBR was tagged N-terminally with biotin, while AtBRCA1, E2FA and E2FB were tagged with Glutathione-S-transferase (GST) at their N-termini. We performed co-immuno precipitations using streptavidin labelled magnetic beads and visualised proteins by Western blot using ExtrAvidin-POD (EA-POD) tagged RBR and GST antibody. RBR showed a clear and specific

interaction with AtBRCA1, compared to the GST control, but was weaker than the positive controls of E2FA (Fig 5). The strength of RBR/E2FB was similar to RBR/E2FA.

Isolation of root material for transcriptome analysis

In order to follow the dynamics underlying the phenotypic changes due to *RBR* silencing we have analysed the *rRbr* line at early time points of development. At 4 days after sowing (das) the organization of the stem cell niche in *rRBr* largely resembles the one in the wild-type control visualized by Lugol staining using differential interference contrast (DIC) microscopy (Fig EV1A). Labelling the cells with EdU (5-ethynyl-2'- deoxyuridine, 6h), however, we could show excess number of columella (CSC) and lateral root cap initials (LRC) in S-phase (Fig EV1B). The number of stem cell layers and the number of cells going through S-phase continued to increase at 6 and 10 das (Fig EV1A and B, respectively). The cell death inducing effect of *RBR* silencing was also detectable from 4 das onwards and the number of dead cells increased by time (Fig EV1C). Germination of seeds, Col-0 and *rRBr*, for the different time points started at the same time under the same conditions and were repeated three times. The phenotypic changes were followed in each experiment via Lugol staining. As the changes occur mainly in the stem cell niche we have dissected the root tips carefully under the microscope and collected material between 20-40mg. RNA isolation and the quality control were carried out according to the manufacture's recommendation (RNA cc. varied, 3-30 µg). The level of *RBR* silencing was determined by qRT-PCR from the 10das sample of each repeat and found to be around 80% of the control at the same time point.

Analysis of micro-array data

cDNA synthesis, labelling and hybridization to ATH1 Affymetrix Chips were performed at ServiceXS (Leiden, The Netherlands). At least, two biological replicas were used for each time point.

Microarray analysis was performed using the Affymetrix package within Bioconductor (www.bioconductor.org). Samples were normalized with the RMA algorithm and differential expression was assessed using the LIMMA package (Smyth, 2004) and the Benjamini and

Hochberg multiple testing correction (Benjamini *et al.*, 2001). In order to identify the common *rRBr* targets through the analysed time frame, samples were clustered in two groups (wild-type and *rRBr*). We defined differentially expressed genes when p-value < 0.01 was combined with a fold change ≥ 1.4.

The level of *RBR* reduction in the microarray samples matched well with the reduction measured by qRT-PCR in the dissected *rBRr* root tips compared to Col-0. No reduction was detectable when RNA was isolated from the entire meristem, confirming that our sample was enriched for cells within the *RCH1* expression domain where *RBR* silencing had taken place.

Gene ontology (GO) overrepresentation analysis was carried out using Fisher Exact Test with FDR correction (p<0.01) and background population Tair10 ATH1 at Virtual Plant 1.3 (Katari *et al.*, 2010). Co-expression networks were obtained from ATTED-II web server (Obayashi *et al.*, 2011).

Analysis of the differentially expressed genes

In total, 99 genes showed significant differential expression between *rRBr* and Col-0 during the studied 3 time points, using the above stringent parameters in statistical data analysis (AppendixTable S1). Most of the genes (82) were up-, and 17 were down-regulated, including *RBR* itself. Gene ontology (GO) analysis uncovered that the up-regulated genes within the *rRBr* set were significantly enriched for nuclear proteins and functionally related to the following major processes; (1) nucleosome and chromosome assembly and organisation (39%), (2) DNA replication (21%) and (3) DNA damage response and DNA repair (16%) (4) cell cycle checkpoint (6%), (Appendix Table S2). To reveal possible links among the genes in the three GO categories, we performed a co-expressional analysis, seeded around a well-characterized member of each cluster; the *HISTONE 2B* (*HTB9,* At3g45980, cluster 1, Appendix Fig S2A), the *RIBONUCLEOTIDE REDUCTASE* (*RNR*) *SMALL SUBUNIT* (*TSO2*, At3g27060, cluster 2, Appendix Fig S2B) and the *BREAST CANCER SUSCEPTIBILITY1* (*AtBRCA1,* At4g21070, cluster 3 Appendix Fig S2C). A large portion (11/27) of the *HISTONE* genes, mainly HISTONE2-type, showed co-expression (Appendix Fig S2A). The replication

related transcripts, the *PROLIFERATING CELL NUCLEAR ANTIGEN 2 (PCNA2)*, the *REPLICON PROTEIN A2* (*RPA2*), alongside some non-annotated transcripts, formed a co-expressional cluster. The *PROLIFERA*, the *STRUCTURAL MAINTENANCE OF CHROMOSOME 6A*, the *DNA POLYMERASE ALPHA* and its *CATALYTIC SUBUNIT* did not fall in this co-expressional cluster but their expression was also consistent with the regulatory function of RBR at the entry of replication (Appendix Fig S2B). Similarly, a large overlap (10 out of 14 transcripts) was found between the *AtBRCA1* co-expressional cluster and the *rRBr* gene set annotated as DNA damage response (DDR), among others the *RECOMBINASE PROTEIN51* (*RAD51*), *POLY(ADP-RIBOSE) POLYMERASE2* (*PARP2*), *GAMMA-IRRADIATION AND MITOMYCIN INDUCED 1* (*GMI1*) (Appendix Fig S2C). Genes involved in cell cycle checkpoint activation, such as the *CYCLIN DEPENDENT KINASE INHIBITORS*, the *KIP-RELATED PROTEIN3* and *5* (*KRP3* and *KRP5*) and *SIAMESE-RELATED4* (*SMR4*) and the related *SMR6*, were also up-regulated. At lower level of statistical stringency, another family member, *SMR5* also showed increased expression in *rRBr*. A large portion (58/82) of the up-regulated genes overlapped with the published dataset of inducible RBR silencing in leaves (Borghi *et al.*, 2010), including all the replication-related genes and part of the AtBRCA1 co-expressional genes (Appendix Table S1).

To relate the *rRBr* transcriptome to upstream and downstream regulatory networks of RBR and to the DNA damage response pathways, we performed a meta-analysis of micro-array experiments. We found a substantial overlap with our *rRBr* and the *CYCD3;1* overexpression (de Jager *et al.*, 2009, Menges *et al.*, 2006) or the *E2Fa-DPa* co-overexpression datasets (de Jager *et al.*, 2009, Menges *et al.*, 2006, Naouar *et al.*, 2009, Vandepoele *et al.*, 2005), mainly representing transcripts confined to the co-expressional clusters described above (Appendix Table S1). Eight out of the ten “BRCA1 co-expressional genes” are expressed in an ATM- and SOG1-dependent manner after gamma-irradiation (Appendix Table S1) and induced by genotoxic agents, such as hydroxyurea (Adachi *et al.*, 2011, Cools *et al.*, 2011) or bleomycin (Yi *et al.*, 2014). The same transcripts are also among

the CYCD3.1 regulated genes, suggesting that these transcripts are commonly regulated by the CYCD3;1-RBR and ATM-SOG1 pathways. In addition, some RBR regulated transcripts are ATM dependent, but independent of SOG1 and CYCD3;1 regulation, raising the possibility of a SOG1-independent pathway.

Expression analysis

RNA was extracted from 5-6 das seedlings or root samples (varied between 50-100) using the RNeasy Mini Kit (Qiagen). cDNA was synthesized with the QuantiTect Reverse Transcription Kit according to the manufacturer's recommendation (http://qiagen.com). Quantitative Real-Time PCR (qRT-PCR) was carried out using SYBR Green Jumpstart reaction mixture (Sigma) on 0,2 µg cDNA. Transcript levels were normalized to *ACTIN2* (*ACT*) level and analysed using Relative Expression Software Tool 2009 (REST 2009, Qiagen). Primer sequences are summarised in Appendix Table S3. Each treatment and mutant analysis was repeated at least twice (biological repeat, n) in different laboratory; the effect of genotoxic agent was controlled by confocal microscopy prior to RNA isolation.

Mutants and their phenotypic analysis

The Arabidopsis thaliana ecotype Landsberg erecta (*35S::CYCD3;1*) line G54 (Dewitte *et al.*, 2003, Riou-Khamlichi *et al.*, 1999) was introgressed to Col-0 to generate Col-0 (*CYCD3;1OE*). F3 batches which were homozygous for the T-DNA insertion and displayed Col-0 inflorescences were identified. PCR-based genotyping was carried out using primers listed in Appendix Table S3.

The influenza HA-tagged E2FB had been previously cloned into the pK7WG2 Gateway vector (Magyar *et al.*, 2005). Transgenic Arabidopsis plants over-expressing the dimerization partner A (DPA; (De Veylder *et al.*, 2002) were transformed with the HA-E2FB constructusing the flower-dip method. Thirteen transgenic T1 lines expressing both transgenes were identified, and a single T-DNA insertion line (line 10/15) for both transgenes was selected and used in this study.

The position of the different *e2fa* mutations is shown in Fig EV5A . The *e2fa-1*, *e2fa-2* mutants (MPIZ_244, GABI-348E09, respectively) were characterized earlier (Berckmans *et al.*, 2011); using a primer combination downstream of the relevant insertions, no mRNA was detected in either of the mutants, hence they did not produce the full-sized E2FA. However, the authors did not exclude that truncated protein could be synthesized. In our preliminary experiments, using a specific E2FA N-terminal-related antibody, indeed we could detect a specific, lower mobility protein in the *e2fa-2* mutant. Based on this, we assumed that *e2fa-1* and *e2fa-2* are loss-of-function rather than null mutants. The truncated *e2fa-1* and *e2fa-2* alleles differ in their 'marked-box' domain but both could dimerize with DPs. Thus, we suggested that the difference in the observed phenotype did not relate to a dominant negative effect sequestering DPs, but rather, the "marked-box' domain plays an important role. The *e2fa-3* mutant was isolated by (Xiong *et al.,* 2013) and described as a null allele. The introgressed *amiRBR;e2fa* mutants were genotyped for the *e2fa* mutations, while RBR silencing was analysed for via qRT-PCR (Fig EV5B).

The presence of *amiRBR* construct in the *amiRBR;brca1* mutants was first pre-screened for the presence of a GFP marker introgressed together with the *amiRBR* construct. The GFP marker was not a direct "readout" for the reduction of the *RBR* level, thus the same (individual) seedlings analysed for cell death were also tested for QC and stem cell maintenance; in addition, we counted the columella cell layers as an indication for extra stem cell division (Fig EV4F and G). EdU labelling on the homozygous F3 batch also confirmed that the *35S$_{pro}$:amiGORBR* (Cruz-Ramirez *et al.*, 2013) transgene was still functional (Fig EV4D). The double mutants were genotyped, and the absence of functional AtBRCA1 was controlled by expressional studies upon MMC treatment (Fig EV5C).

To follow whether spontaneous cell death upon RBR silencing depends on the SOG1 function, we transformed homozygous *sog1-1* plants (Preuss & Britt, 2003) with the *35S$_{pro}$:amiGORBR* construct (Cruz-Ramirez *et al.*, 2013). More than 20 independent transformants were generated, genotyped by sequencing of the *sog1-1* locus and analysed

for *RBR* silencing (Fig EV6C).

Cell death phenotype was quantified by scoring the number of dead cells in the QC, columella and lateral root cap stem and daughter cells. Parallel, we quantified the area of dead cells also in the proximal meristem. As this assay was very sensitive and was dependent on the age of the seedlings (5 to 6 days), the length of storage of the MMC, the affected area especially, in the case of the *Atbrca1* mutants differed from experiment to experiment. For this reason, cell death was quantified in each experiment from each line and the control at least on 15 seedlings. Though the relative values between different experiments varied, the ratio of cell death area comparing the control and mutants was nearly constant (Fig EV3E).

Protein complex isolation, LC-MS/MS identification and label free MS quantitation

Sample preparation

E2FA-GFP *(pE2FA:gE2FA-GFP)* and *p35:GFP* (Magyar *et al.*, 2012) seeds were germinated in normal growth conditions. For genotoxic treatment 6 das seedlings were transferred to liquid MS media with or without MMC (20 µg/ml) for 16 hours. 150-200 seedlings were harvested and processed. Total proteins were extracted as described earlier (Henriques *et al.*, 2010). The total protein extracts (4mg/IP) were immune-purified using anti-GFP antibody coupled with very small magnetic beads (MACS® Technology, Miltenyi) digested in column with trypsin, and analysed in a single run on the mass spectrometer (Hubner *et al.*, 2010).

Mass spectrometry

The resulting peptide mixture first was desalted (Omix C18 100 ul tips, Varian) then analysed by LC-MS/MS using a nanoflow RP-HPLC (Lc program: linear gradient of 3-40 % B in 100 min, solvent A: 0.1% formic acid in water, solvent B: 0.1% formic acid in acetonitrile) on-line coupled to a linear ion trap-Orbitrap (Orbitrap-Elite, Thermo Fisher Scientific) mass spectrometer operating in positive ion mode. Data acquisition was carried out in data-dependent fashion; the 10 most abundant, multiply charged ions were selected from each

MS survey for MS/MS analysis (MS spectra were acquired in the Orbitrap, and CID spectra in the linear ion trap).

Data interpretation

Raw data were converted into peak-lists using the in-house PAVA software (Guan *et al.*, 2011) and searched against the Swissprot database (version:16/04/2015, 548208 proteins) using the Protein Prospector search engine (v5.15.1) with the following parameters: enzyme: trypsin with maximum 1 missed cleavage; mass accuracies: 5 ppm for precursor ions and 0.6 Da for fragment ions (both monoisotopic); fixed modification: carbamidomethylation of Cys residues; variable modifications: acetylation of protein N-termini; Met oxidation; cyclization of N-terminal Gln residues allowing maximum 2 variable modifications per peptide. Acceptance criteria: minimum scores: 22 and 15; maximum E values: 0.01 and 0.05 for protein and peptide identifications, respectively. Another database search was also performed using the same search and acceptance parameters except that Uniprot.random.concat database (version:16/04/2015) was searched with Arabidopsis thaliana species restriction (52524 proteins) including additional proteins identified from the previous Swissprot search (protein score>50). False discovery rate was estimated using peptide identifications representing randomized proteins (2* #of random IDs/ total peptide IDs) = 2 times number of random IDs divided by peptide IDs.

Spectral counting was used to estimate relative abundance of individual proteins in the MMC-treated and control samples: peptide counts of the individual proteins were normalized to the total number of peptide identifications in each sample, then these normalised peptide counts were compared in the two samples. The median of these normalized peptide count ratios was 0.9715, therefore, the ratios were corrected with this value.

Reference to Supplementary Methods

Adachi S, Minamisawa K, Okushima Y, Inagaki S, Yoshiyama K, Kondou Y, Kaminuma E, Kawashima M, Toyoda T, Matsui M, Kurihara D, Matsunaga S, Umeda M (2011) Programmed induction of endoreduplication by DNA double-strand breaks in Arabidopsis. Proc Natl Acad Sci U S A 108: 10004-9

Benjamini Y, Drai D, Elmer G, Kafkafi N, Golani I (2001) Controlling the false discovery rate in behavior genetics research. Behav Brain Res 125: 279-84

Berckmans B, Vassileva V, Schmid SP, Maes S, Parizot B, Naramoto S, Magyar Z, Alvim Kamei CL, Koncz C, Bogre L, Persiau G, De Jaeger G, Friml J, Simon R, Beeckman T, De Veylder L (2011) Auxin-dependent cell cycle reactivation through transcriptional regulation of Arabidopsis E2Fa by lateral organ boundary proteins. Plant Cell 23: 3671-83

Borghi L, Gutzat R, Futterer J, Laizet Y, Hennig L, Gruissem W (2010) Arabidopsis RETINOBLASTOMA-RELATED is required for stem cell maintenance, cell differentiation, and lateral organ production. Plant Cell 22: 1792-811

Cools T, Iantcheva A, Weimer AK, Boens S, Takahashi N, Maes S, Van den Daele H, Van Isterdael G, Schnittger A, De Veylder L (2011) The Arabidopsis thaliana checkpoint kinase WEE1 protects against premature vascular differentiation during replication stress. Plant Cell 23: 1435-48

Cruz-Ramirez A, Diaz-Trivino S, Wachsman G, Du Y, Arteaga-Vazquez M, Zhang H, Benjamins R, Blilou I, Neef AB, Chandler V, Scheres B (2013) A SCARECROW-RETINOBLASTOMA protein network controls protective quiescence in the Arabidopsis root stem cell organizer. PLoS Biol 11: e1001724

Culligan KM, Robertson CE, Foreman J, Doerner P, Britt AB (2006) ATR and ATM play both distinct and additive roles in response to ionizing radiation. Plant J 48: 947-61

de Jager SM, Scofield S, Huntley RP, Robinson AS, den Boer BG, Murray JA (2009) Dissecting regulatory pathways of G1/S control in Arabidopsis: common and distinct targets of CYCD3;1, E2Fa and E2Fc. Plant Mol Biol 71: 345-65

De Veylder L, Beeckman T, Beemster GT, de Almeida Engler J, Ormenese S, Maes S, Naudts M, Van Der Schueren E, Jacqmard A, Engler G, Inze D (2002) Control of proliferation, endoreduplication and differentiation by the Arabidopsis E2Fa-DPa transcription factor. EMBO J 21: 1360-8

Dewitte W, Riou-Khamlichi C, Scofield S, Healy JM, Jacqmard A, Kilby NJ, Murray JA (2003) Altered cell cycle distribution, hyperplasia, and inhibited differentiation in Arabidopsis caused by the D-type cyclin CYCD3. Plant Cell 15: 79-92

Guan S, Price JC, Prusiner SB, Ghaemmaghami S, Burlingame AL (2011) A data processing pipeline for mammalian proteome dynamics studies using stable isotope metabolic labeling. Mol Cell Proteomics 10: M111 010728

Henriques R, Magyar Z, Monardes A, Khan S, Zalejski C, Orellana J, Szabados L, de la Torre C, Koncz C, Bogre L (2010) Arabidopsis S6 kinase mutants display chromosome instability and altered RBR1-E2F pathway activity. EMBO J 29: 2979-93

Hubner NC, Bird AW, Cox J, Splettstoesser B, Bandilla P, Poser I, Hyman A, Mann M (2010) Quantitative proteomics combined with BAC TransgeneOmics reveals in vivo protein interactions. J Cell Biol 189: 739-54

Katari MS, Nowicki SD, Aceituno FF, Nero D, Kelfer J, Thompson LP, Cabello JM, Davidson RS, Goldberg AP, Shasha DE, Coruzzi GM, Gutierrez RA (2010) VirtualPlant: a software platform to support systems biology research. Plant Physiol 152: 500-15

Kobayashi K, Suzuki T, Iwata E, Nakamichi N, Suzuki T, Chen P, Ohtani M, Ishida T, Hosoya H, Muller S, Leviczky T, Pettko-Szandtner A, Darula Z, Iwamoto A, Nomoto M, Tada Y, Higashiyama T, Demura T, Doonan JH, Hauser MT et al. (2015) Transcriptional repression by MYB3R proteins regulates plant organ growth. EMBO J

Magyar Z, De Veylder L, Atanassova A, Bako L, Inze D, Bogre L (2005) The role of the Arabidopsis E2FB transcription factor in regulating auxin-dependent cell division. Plant Cell 17: 2527-41

Magyar Z, Horvath B, Khan S, Mohammed B, Henriques R, De Veylder L, Bako L, Scheres B, Bogre L (2012) Arabidopsis E2FA stimulates proliferation and endocycle separately through RBR-bound and RBR-free complexes. EMBO J 31: 1480-93

Menges M, Samland AK, Planchais S, Murray JA (2006) The D-type cyclin CYCD3;1 is limiting for the G1-to-S-phase transition in Arabidopsis. Plant Cell 18: 893-906

Naouar N, Vandepoele K, Lammens T, Casneuf T, Zeller G, van Hummelen P, Weigel D, Ratsch G, Inze D, Kuiper M, De Veylder L, Vuylsteke M (2009) Quantitative RNA expression analysis with Affymetrix Tiling 1.0R arrays identifies new E2F target genes. Plant J 57: 184-94

Obayashi T, Nishida K, Kasahara K, Kinoshita K (2011) ATTED-II updates: condition-specific gene coexpression to extend coexpression analyses and applications to a broad range of flowering plants. Plant Cell Physiol 52: 213-9

Preuss SB, Britt AB (2003) A DNA-damage-induced cell cycle checkpoint in Arabidopsis. Genetics 164: 323-34

Riou-Khamlichi C, Huntley R, Jacqmard A, Murray JA (1999) Cytokinin activation of Arabidopsis cell division through a D-type cyclin. Science 283: 1541-4

Smyth GK (2004) Linear models and empirical bayes methods for assessing differential expression in microarray experiments. Stat Appl Genet Mol Biol 3: Article3

Vandepoele K, Vlieghe K, Florquin K, Hennig L, Beemster GT, Gruissem W, Van de Peer Y, Inze D, De Veylder L (2005) Genome-wide identification of potential plant E2F target genes. Plant Physiol 139: 316-28

Xiong Y, McCormack M, Li L, Hall Q, Xiang C, Sheen J (2013) Glucose-TOR signalling reprograms the transcriptome and activates meristems. Nature 496: 181-6

Yi D, Alvim Kamei CL, Cools T, Vanderauwera S, Takahashi N, Okushima Y, Eekhout T, Yoshiyama KO, Larkin J, Van den Daele H, Conklin P, Britt A, Umeda M, De Veylder L (2014) The Arabidopsis SIAMESE-RELATED Cyclin-Dependent Kinase Inhibitors SMR5 and SMR7 Regulate the DNA Damage Checkpoint in Response to Reactive Oxygen Species. Plant Cell 26: 296-309

Yoshiyama K, Conklin PA, Huefner ND, Britt AB (2009) Suppressor of gamma response 1 (SOG1) encodes a putative transcription factor governing multiple responses to DNA damage. Proc Natl Acad Sci U S A 106: 12843-8

Legends to Appendix Figures and Tables

Appendix Fig S1. Elevated level of AtBRCA1 is not sufficient to induce cell death response.

(**A)** Accumulation of AtBRCA1-10xmyc protein after 24h β-estradiol (5 μM) induction (+) compared to the non-induced control (-). * indicates lines 3, 4, 5 and 7 used for microscopical studies.

(**B**) No spontaneous cell death response was detected after 24h β-estradiol induction, arrow indicates QC position.

Appendix Fig S2. Co-expression modules of differentially expressed transcripts.

Three co-expression modules created by ATTED-II centred around **(A**) Histone HTB9 (At3g45980), (**B**) TSO2 (At3g27060) and (C) AtBRCA1 (At4g21070). Solid black edges connecting the genes indicate co-expression and brown edges refer to conserved co-expression between Arabidopsis and at least one of three mammalian species (human, mouse and rat) used for comparison. The three Histone highlighted with a black box can form a connection between the overlapping two clusters.

Appendix Table S1. Differentially expressed genes upon RBR silencing comparing the transcriptome of *rRBr* and Col-0

(**A** and **B**) Annotation and (**C**) locus of up-and downregulated transcripts. Upregulated genes are ordered according to the adjusted p-value (**F**), while downregulated genes are listed according to the level of changes (**D**).

(**D**) Fold change (FC) threshold (>1.4) determining differential expression.

(**E**) Average intensity

(**F**) Adjusted p-value for multiple testing correction using Benjamini-Hochbert approach

(**G**) Co-expressional analysis using ATTED-II centred around HTB9, At3g45980 (A); TSO2, At3g27060 (B) and At4g21070=AtBRCA1 (C). Labelling (A), (B) and (C) refers to images in Appendix Fig S2. Colour indicates GO ontology clusters blue colours refers to DNA repair (column **I**), while red colour illustrates DNA replication (columns **H**).

(**H**) GO ontology cluster; Nucleosome assembly: GO0006334

(**I**) GO ontology cluster DNA repair and GO0006281 and GO0000724, coloured blue, if overlaps with co-expressional category centred around AtBRCA1:

(**J**) GO ontology cluster: DNA dependent DNA replication, GO0006261, labelled red, if overlaps with co-expressional category centred around TSO2.

(**K**) Cell-cycle related GO clusters: GO0010389, GO0051726

Genes showing differential expression (**L**) in *sog1-1* (Yoshiyama *et al.*, 2009) and (**M**) *atm-2* (Culligan *et al.*, 2006) mutants.

(**N**) Genes harbouring a potential E2F motif (8bp), using prediction published by Naouar *et al*, 2009, Table S4) in a 1-kb promoter region.

Overlapping differentially expressed genes to (**O**) *CYCD3OE* (de Jager *et al.*, 2009), (**P**) *E2FA-DPaOE* (Naouar *et al.*, 2009) and (**Q-X**) inducible *RBR* RNAi line (Borghi et al, 2010), the induction time and values refer to the article.

Appendix Table S2. Enrichment of Gene Ontology (GO) terms of differentially expressed genes comparing the transcriptome of *rRBr* and Col-0

Appendix Table S3. List of primers used in this study

Appendix Table S4. Label free MS quantitation of E2FA interaction with RBR, DPA and DPB with and without MMC treatment
Seedlings with GFP-tagged E2FA (7das) were treated with and without MMC for 16h, GFP-pull downs were analysed by MS and E2FA, RBR, DPA, DPB were quantitated label-free.

Appendix Table S5. Interaction of E2FA and E2FB with DREAM complex components
Seedlings expressing either GFP-tagged E2FA or E2FB and GFP (7 das) were collected. Pull-downs were performed and analysed by LC-MS/MS. Identified DREAM complex components (Kobayashi *et al.*, 2015) are shown by the number of unique peptides and sequence coverage. None of the identified peptides were detected in the control expressing GFP alone. *representative result from independent experiments (n>10).

Appendix Figure S1

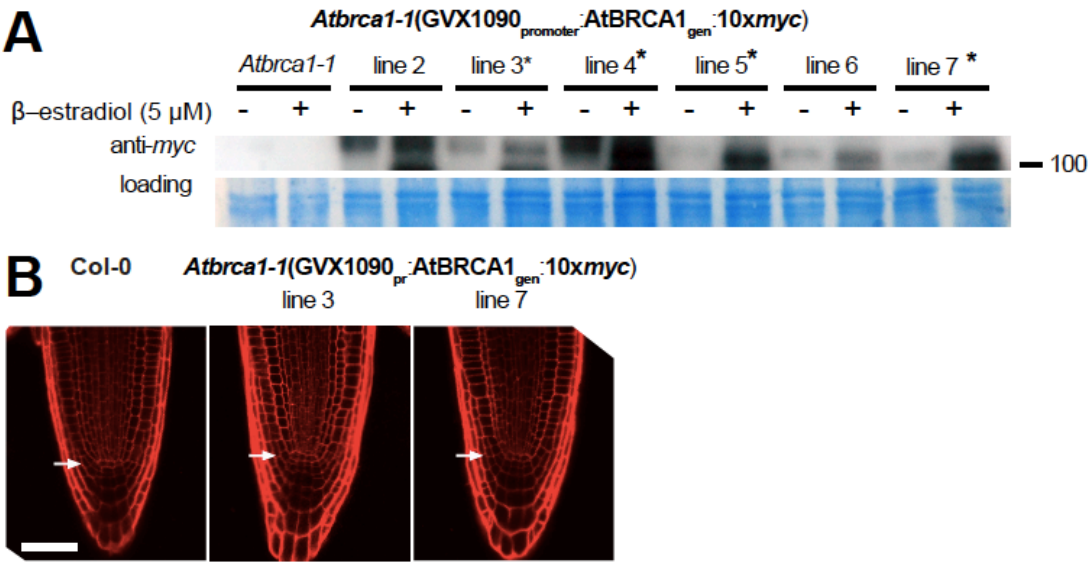

Appendix Figure S2

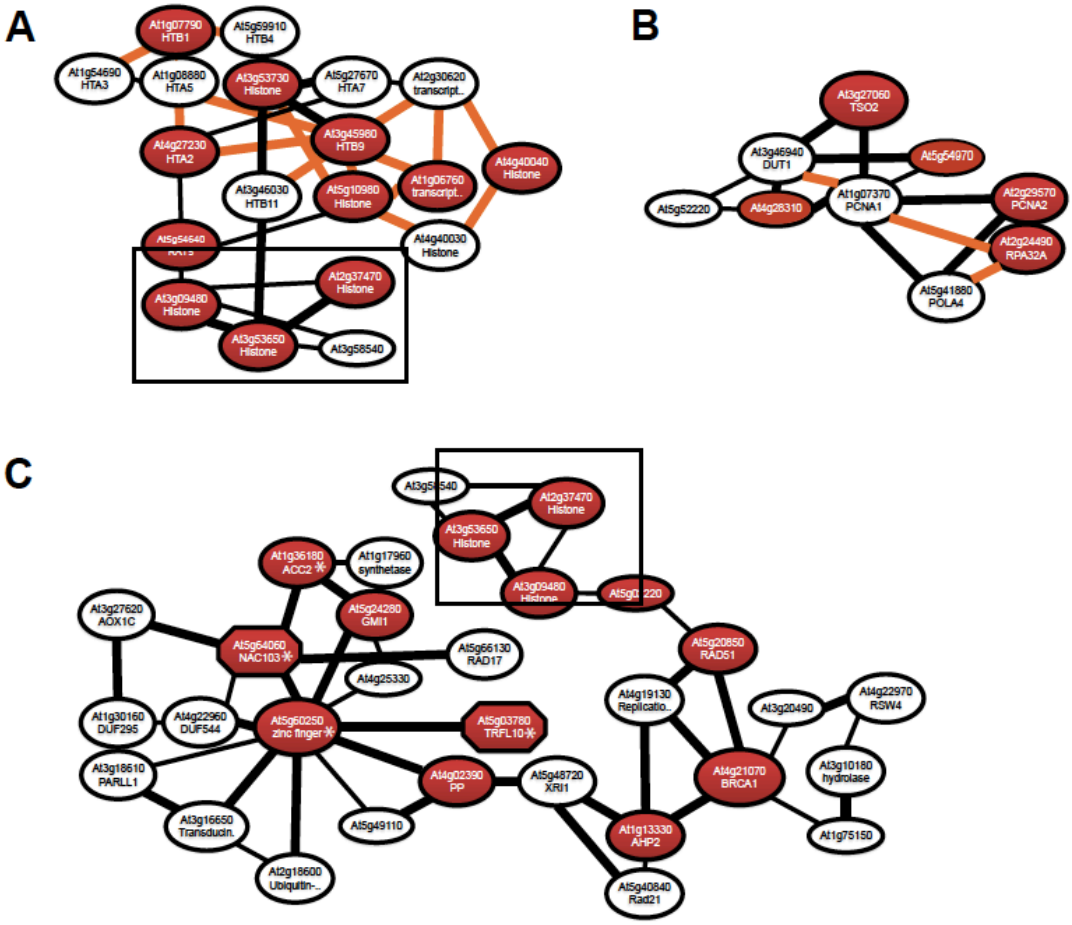

Appendix Table S2

Enrichment of Gene Ontology (GO) terms of differentially expressed genes

	GO term	GO ID
Up-regulated		
	Nucleosome assembly	GO:0006334
	Chromatin organization	GO:0006325
	Chromosome organization	GO:0051276
	Nucleosome	GO:0000786
	DNA binding	GO:0003677
	Cellular component organization at cellular level	GO:0071842
	Nucleus	GO:0005634
	DNA metabolic process	GO:0006259
	DNA repair	GO:0006281
	Response to DNA damage stimulus	GO:0006974
	Response to ionizing radiation	GO:0010212
	Cellular process	GO:0009987
	DNA-dependent ATPase activity	GO:0008094
	Cyclin-dependent protein kinase inhibitor activity	GO:0004861
Down-regulated		
	Regulation of cell cycle	

Appendix Table S3
Primers used in this study

Gene / primer name	Accession no. / sequence
A. Chromatin immunoprecipitation	
At4g21070	**AtBRCA1**
BRCA1F	gtttcatcgcagatcgttca
BRCA1R	ttgcaagatttgaacccatt
BRCA2F	taggggcaaaacgaaaattg
BRCA2R	agatgacgaagcgtgtcctt
BRCA3F	ttctcttgatttcagtgcgtgt
BRCA3R	aatcatcaaactgcaaacttagg
At1g07370	**PCNA1**
PCNA4F	aatgaccaaaaatatccatccaa
PCNA4R	cggctattttggaaagtgga
IR	**At3g03660-70**
IR1F	cattgaacacctattggtaggaa
IR1R	actgttttggtgccagattttcag
B. qRT-PCR	
At3g18780	**ACTIN2**
qActinF	CGCTGACCGTATGAGCAAAG
qActinR	TTCATGCTGCTTGGTGCAA
At3g12280	**RETINOBLASTOMA-RELATED**
qRBRF2	ATAATAAGCCTGAAGGTCAATGTC
qRBRR2	TAAACATTGTGCACTGCAGATACT
At2g21070	**BREAST CANCER ASSOCIATED-1**
qBRCA1F2	TCATGGGAGATTTCGAGCTT
qBRCA1R2	ATTTAGCCAAGGCTTCAGCA
qBRCA330F	TGGAAGATGCTTCTGGGATT
qBRCA480R	CTCGTTCCTCTTGGATGCTC
qBRCA2210F	TGCACTCTCAGCCTAAACAAG
qBRCA2380R	ACTCCAGACAGTTCCGCAAA
At4g02390	**POLY-(ADP-RIBOSE) POLYMERASE2**
qPARP2F	TCGAGAGCTGTTGAAGCTGA
qPARP2R	GGAGCTATTCGCAGACCTTG
At1g09200	**HISTONE3.1**
qH3.1F	AGCAGACGGCTAGGAAATCA
qH3.1R	CAACAGTTCCGGGTCTGAAT
At5g02220	**SMR4, SIAMESE-RELATED 4**
At5g02220F	GGCGTCTGTTTGTCCACC
At5g02220R	CCCTAAACATGTATCTACAGAGAAG
At1g07500	**SMR5, SIAMESE-RELATED 5**
At1g07500F	AAACTACGACGACGGAGATACG
At1g07500R	GCTACCACCGAGAAGAACAAGT
At5g24280	**GMI, GAMMA-IRRADIATION AND MITOMYCIN C INDUCED**
qGMIF	CCTCATTGTTGGATCCTTGG
qGMIR	TCCCAGCATAAGCTCCTCTC
At5g20850	**RAD51**
qRAD51F	TTGCTGGTCCCCAATTTAAG
qRAD51R	CAAACATGGCGAGCTTATCA
At5g10440	**CYCD4.2**
qCYCD4.2F	GCAGTGACACCGTGCTCTTA
qCYCD4.2R	ACTGCAGCAGCAATCTCTGA

At5g24240	**PHOSPHOTIDYLINOSITOL 3 and 4-KINASE**
qPIPF	GCACTATGGCTTCTGCATCA
qPIPR	GCACTATGGCTTCTGCATCA

C. Genotyping

brca1-1	**At4g21070**
BRCA1-1F(LP)	agagtcgctttgttcctgattc
BRCA1-1R(RP)	gatgctcggcccttccta
LBb1.3	attttgccgatttcggaac
brca1-1/brca1-3	
brca1koF	tggagaggatgggaagagaa
brca1koR	cactgcctttgtttcgttca
e2fb-2	**At5g22220**
E2FB-RP	gtgcctttacagctatcagcg
E2FB-LP	ttggattccttccatttgatg
LBb1.3	attttgccgatttcggaac

Col-0*(CYCD3OE)*	
Forward(CaMV35S)	TCCGGAAACCTCCTCGGA (CaMV35S)
Reverse	GCTGCGGCAACTACTGATGG
CYCD3;1 FLANKING	
Forward	TAAACTCAGCCGTCCGATCAC
Reverse	TGAGATTCATGGTGATAACCTCG

D. Cloning:

pBRCAF1	gtttcatcgcagatcgttca
pBRCAR2	tttcgatcttcactcagag
gBRCA1F1	ATGGCGGACACTAGTCACC
gBRCA1R1	TATCAAGACTAAAATTTGGC

BiFC cDNA	
BRCA1cDNAF	ggggacaagtttgtacaaaaaagcaggctgta* (vector) *TGGCGGACACTAGTCACCTGGAGAGGATGGGAAGAG
BRCA1cDNAR	ggggaccactttgtacaagaaagctgggtt*(vector) *TATCAAGACTAAAATTTGGCAACCTGCAATAGAAT** **CCAAAACCCATCCAAAACCC

Appendix Table S4

Label free MS quantitation of E2FA interaction with RBR, DPA and DPB -/+ MMC

Identified DREAM-complex proteins		Number of unique/total peptide identifications			
Name	AGI number	E2FA untreated		E2FA treated (MMC)	
		unique	total	unique	total
E2FA	AT2G36010	12	28	9	23
RBR1	AT3G12280	31	44	32	52
DPB	AT5G03415	8	18	6	13
DPA	AT5G02470	7	11	6	9

Appendix Table S5

Interaction of E2FA or E2FB with DREAM complex components

Identified DREAM-complex proteins		UNIQUE PEPTIDES/ % COVERAGE	
Name	AGI number	E2FA*	E2FB*
E2FA	AT2G36010	12/28.2%	-
E2FB	AT5G22220	-	17/44.3%
RBR1	AT3G12280	28/31.8%	37/37.2%
DPB	AT5G03415	9/30.9	7/25.2%
DPA	AT5G02470	6/19.2%	5/18.2%
ALY3	AT3G21430	-	2/4.3%
TCX5	AT4G29000	-	3/3%
MSI1	AT5G58230	-	3/8.7%

*Representative result from independent experiments (n>10)